

#### 4. SERPENTINIZED, RESIDUAL MANTLE PERIDOTITES FROM THE M.A.R. MEDIAN VALLEY, ODP HOLE 670A (21°10'N, 45°02'W, LEG 109): PRIMARY MINERALOGY AND GEOTHERMOMETRY<sup>1</sup>

Thierry Juteau,<sup>2</sup> Emmanuel Berger,<sup>3</sup> and Mathilde Cannat<sup>2</sup>

##### ABSTRACT

During Leg 109 of the Ocean Drilling Program, about 100 m of serpentinized peridotites were drilled on the western wall of the M.A.R. axial rift valley, 45 km south of the Kane Fracture Zone. The present study reports petrological and mineralogical data obtained from 29 small pieces of these ultramafic rocks, including about 60% serpentinized harzburgites, 26% serpentinized lherzolites, 14% serpentinized dunites, and one sample of olivine websterite. Modal analyses show that all these rocks are plagioclase-free four-phase peridotites equilibrated in the spinel lherzolite facies. The estimated average modal composition of the sample set is about 80% olivine, 14% opx, 5% cpx, and 1% spinel, that is, a cpx-poor lherzolite.

The well developed porphyroclastic structures and mineralogical characteristics of these rocks indicate their affinity with the group of residual mantle tectonites, among the abyssal peridotites. Features typical of magmatic cumulates are lacking.

The high contents in Al<sub>2</sub>O<sub>3</sub> of the cpx (average 5.4%) and of the opx (average 4.3%) porphyroclasts, the low Cr# of the spinels (average 22.9%), and the rather high content in modal cpx (about 5%), indicate a moderate percentage of melting, of the order of 10%–15%. Site 670 peridotites plot close to the least depleted mantle rocks collected in the oceans in most diagrams used to define the average trend of the ocean-floor peridotites.

Microprobe traverses across the cores of the exsolved opx and cpx porphyroclasts permitted the recalculation of the magmatic compositions of these pyroxenes: the "primitive" opx were equilibrated at about 1300°C, probably at the end of the main melting episodes, whereas the "primitive" cpx show lower equilibration temperatures, at about 1200°C, reflecting a more complex thermal history. The subsolidus evolution is well recorded, from 1200°C to about 950°C, by the exsolved pyroxenes and the olivine and spinel phases. Unusually high blocking temperatures, close to 1000°C, indicate that the peridotite body was cooled very rapidly between 1000°C and the beginning of serpentinization.

Oxygen fugacities, calculated for 10 kb and at the blocking temperatures indicated by the olivine/spinel geothermometer, are close to the usual fugacities calculated in oceanic peridotites and basalts (of the order of 10<sup>-11</sup> to 10<sup>-12</sup>, on the QFM buffer).

Site 670 peridotites have compositions close to those of the peridotites collected in the Kane Fracture Zone area, and obviously belong to the moderately depleted mantle peridotites which characterize abyssal peridotites collected away from mantle plumes and oceanic islands. In particular, they differ from the highly residual harzburgites collected along the M.A.R. over the Azores bulge.

##### INTRODUCTION

There is growing evidence that extension at oceanic spreading centers is accommodated by two main processes: magmatic activity, and tectonic stretching of the lithosphere. The fundamental differences in morphology observed at fast and slow spreading centers probably reflect the balance between these two processes. At fast spreading centers, the magma budget is high and magmatism alone is continuous enough to accommodate extension by addition of new material at the axis. At slow spreading centers, surface magmatism is obviously less continuous, and extension is accommodated at least pro parte by tectonic stretching and extension of the lithosphere. Along the M.A.R. axis, short wavelength variations in the magmatic/tectonic activity were recently documented at 23°N (Karson et al., 1987), indicating a great variability in magma supply vs. tectonic extension at slow spreading rates.

As a consequence, deep plutonic rocks of the crust and serpentinized peridotites from the mantle can be exposed on the ocean floor, not only at ridge/transform intersections or along fracture zones, but also in nonfracture zone settings along slow spreading ridge segments (see Juteau, Cannat, and Lagabrielle, this volume). The exact mechanism of exposure of these deep-level rocks remains controversial. In any case, their outcrops on the ocean floor provide unique windows into the subaxial upper mantle and the primary magmatic products that consolidate at depth.

Most models for the formation of oceanic crust propose that a molten basaltic fraction is extracted from the mantle and emplaced at mid-oceanic ridges, to form the various rocks of the crust. Recent studies in the North Atlantic Ocean have shown that regional variations in basalt chemistry correspond to variations in the modal and chemical composition of fracture zone and nonfracture zone mantle peridotites from the same regions (Dick et al., 1984; Michael and Bonatti, 1985), and may be ascribed to the amount of basaltic melt that has been extracted from the peridotites.

The aim of this paper is to examine how modal and mineralogical characteristics of the mantle peridotites cored at Site 670 compare with those of other mantle peridotites from the M.A.R. in the North Atlantic and fit within the regional trends. It is also our purpose to get some insights on the

<sup>1</sup> Detrick, R., Honnorez, J., Bryan, W. B., Juteau, T., et al., 1990. *Proc. ODP, Init. Repts.*, 106/109: College Station, TX (Ocean Drilling Program).

<sup>2</sup> Groupement de Recherche "Genèse et Evolution des Domaines Océaniques," Université de Bretagne Occidentale, 6 Avenue Le Gorgeu, 29287 Brest Cedex, France.

<sup>3</sup> Ecole Nationale Supérieure des Mines de Paris, Centre de Géologie Générale et Minière, 35 rue Saint-Honoré, 77305 Fontainebleau Cedex, France.

thermal history and degree of partial melting experienced by these rocks during their ascent and emplacement on the ocean floor.

**GEOLOGICAL SETTING**

Site 670 is located at 23°10.00'N, 45°01.93'W in 3625 m of water, on the sloping west wall of the median valley. It lies about 45 km south of the Kane Fracture Zone and 5–6 km to the west of the M.A.R. axis (Karson et al., 1987) (Fig. 1). The floor of the median valley east of Site 670 belongs to a bathymetrically and magnetically “anomalous” ridge segment extending from about 23°08'N to 23°18'N. In this segment, the central magnetic anomaly appears shifted to the west, and the

volcanic axis is deep and poorly defined, compared to its development further to the north or to the south (Purdy et al., 1978; Detrick et al., 1985). In addition, seismic studies have shown that a drastic change in crustal thickness occurs along this segment, from a “normal” crustal thickness to the south, to a thinned crust to the north (Detrick and Purdy, 1980; Cormier et al., 1984). Karson et al. (1987), who conducted a submersible survey along the median valley between the Kane F.Z. and Site 648, interpret this zone as a “zero-offset transform” located at the boundary between two magmatic cells: the submersible study has confirmed the lack of a well-developed median valley, the presence of high scarps and asymmetrical fault-bounded blocks across the entire area, and the absence of any neovolcanic zone or hydrothermal activity. To the north, serpentinized peridotites, gabbros, and greenstones are the dominant lithologies on the west wall of the median valley (Fig. 1), approaching the Kane F.Z. (Bryan et al., 1981; Karson and Dick, 1983; Karson et al., 1987). To the south, Melson et al. (1968) have shown that the median valley walls are composed of greenstones and weathered basalts.

At Site 670, serpentinized peridotites are exposed over more than 1 km in width (Karson et al., 1987). Hole 670A washed through 6.4 m of sediments and drilled 86.1 m into ultramafic rocks, from which a total of 6.12 m of core was recovered.

**PETROGRAPHIC DESCRIPTION OF THE SAMPLES**

We analyzed the 29 samples in our possession in thin sections, under a regular microscope, and selected 9 samples for detailed investigation of their primary mineralogy (Fig. 2).

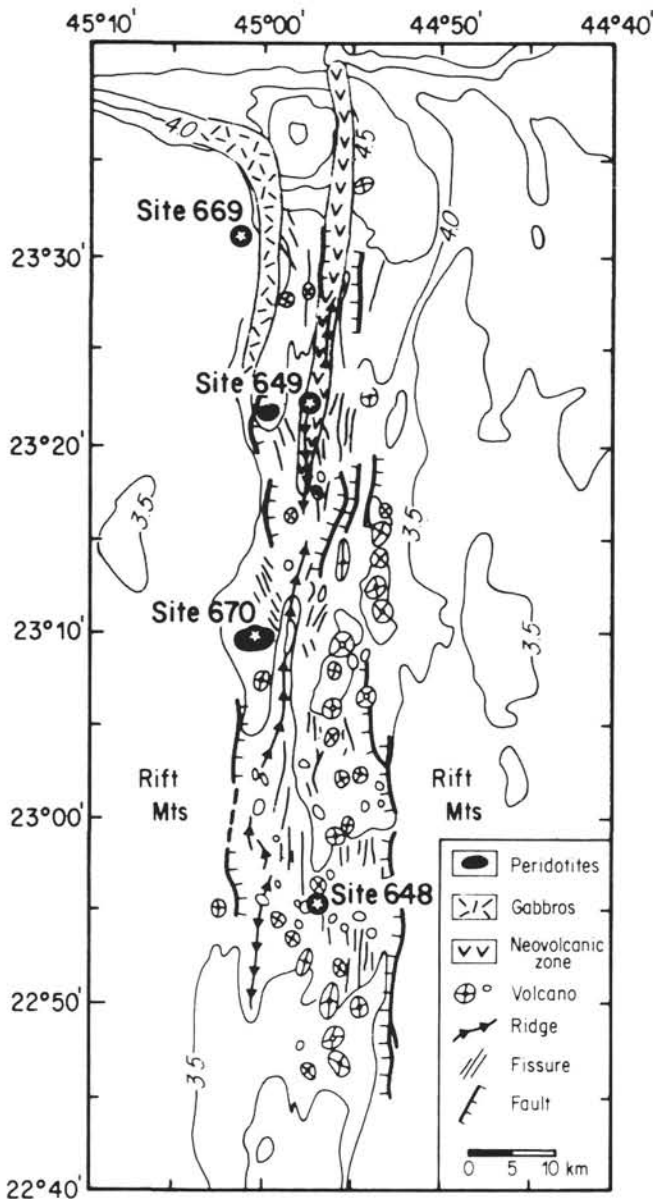


Figure 1. Geological and structural sketch map of the M.A.R. axial valley from 22°40'N (bottom) to the intersection with the Kane Fracture Zone (top). The main sites drilled during Legs 106 and 109 are indicated. Peridotite and gabbro outcrops and neovolcanic zones mainly after submersible surveys (Karson and Dick, 1983; Karson et al., 1987). Bathymetry and tectonic features from Detrick et al. (1985), Purdy and Detrick (1986), and Pockalny et al. (in press).

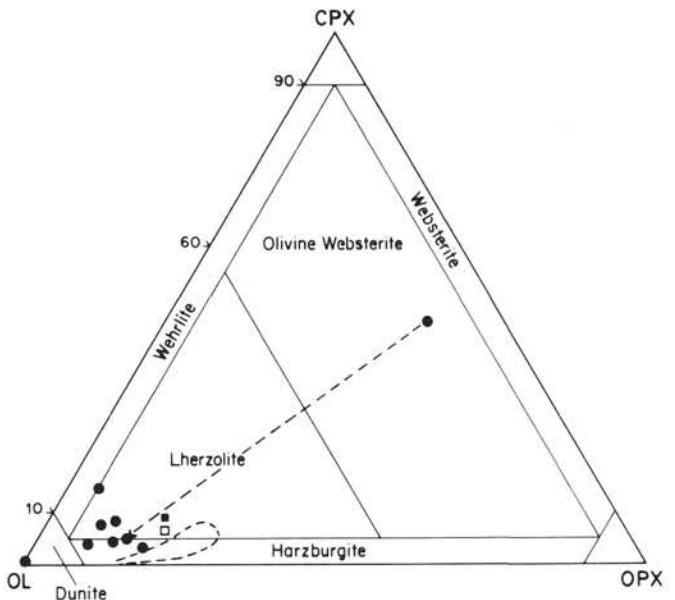


Figure 2. Serpentine-free compositions of the nine selected samples studied in this paper, plotted in the modal ternary ultramafic diagram. The collection consists of one dunite, four harzburgites, three lherzolites, and one olivine websterite. The cross indicates the calculated average composition of the whole sample set (see text). It is a cpx-poor four-phase lherzolite. The dashed line indicates the field of the North-Atlantic peridotites, after Michael and Bonatti (1985). Open square and black square = normative compositions of the Tinaquillo peridotite and pyrolite of Ringwood (1966), respectively (taken from Jaques and Green, 1980). The normative composition of the 8 kb melting point is from Takahashi and Kushiro (1983).

The criteria for this selection are as follows: (1) adequate representation of the 4 petrographic facies recognized as protoliths in the 29 samples of serpentinitized ultramafic rocks of our collection (4 dunites, 17 harzburgites, 7 lherzolites, and 1 olivine websterite); (2) even distribution of the selected samples in the cored section; and (3) limited serpentinitization (less than 78%). Table 1 gives the modal composition of the 9 selected samples (inferred protoliths: 1 dunite, 4 harzburgites, 3 lherzolites, and 1 olivine websterite), and their approximate stratigraphic position in the drilled section.

The modal analyses presented in Table 1 were obtained by counting a minimum of 1000 points per thin section, on a grid spacing of 0.05 mm. The mineral phases taken into account are olivine (ol), orthopyroxene (opx), clinopyroxene (cpx), and Cr-spinel (sp) for the primary phases, and serpentine, bastite, talc, tremolite-actinolite, and magnetite for the secondary phases. Reconstructed primary modes were calculated with the following conventions:

1. Mesh-textured serpentine and associated magnetite grains were assigned to primary olivine.

2. Bastite pseudomorphs and associated talc were assigned to primary opx.

3. Tremolite-actinolite clusters or rims were assigned to both primary cpx and opx.

4. Magnetite developed at the margins of Cr-spinels was assigned to primary spinel.

The primary mineralogical modes were calculated assuming no volume increase during serpentinitization. As pointed out by several authors, this assumption is probably not true. Thus, the reconstructed compositions overestimate olivine and opx, and underestimate cpx. This means that the primary modal compositions proposed in Table 1 give a minimum estimate of the cpx content in the peridotites. An estimated cpx content calculated for a volume increase of 30% during serpentinitization is also shown in Table 1.

Because of the poor rate of recovery (1.2%–17%) and the small size of the samples, the relationships between these various petrographic facies along the core section are not well visible. However, there is no systematic distribution of these facies at the scale of the drilled hole. The cpx appears to concentrate in clusters 1–10 mm across, in association with opx. These cpx-rich clusters are elongated in the foliation of the samples and are found all through the cored section. Thin sections including such clusters yield the most lherzolitic compositions.

All the studied samples are tectonites: elongate spinel and opx grains define a foliation and a lineation, often visible

directly on the cored section (Pl. 1, Fig. 5). Under microscope, the microstructure of these peridotites is of the "elongated porphyroclastic" type (Mercier and Nicolas, 1975). A detailed study of the microstructures and associated fabrics developed in these rocks is given in Cannat et al. (this volume). Here is a brief description of the nine samples selected for microprobe analysis:

#### Serpentinitized dunite (Sample 7R-1, 7–10 cm)

This rock is mainly made of olivine grains appearing as residual cores of primary porphyroclasts (up to 2 mm in size), or recrystallized grains (0.2–0.4 mm in size), isolated by a mesh-textured net of serpentine. Undulatory extinctions are common. Two small cpx crystals (< 0.3 mm) are visible, one of them exhibiting thin opx exsolution lamellae. Tiny (0.1 mm) reddish-brown spinel crystals are scarce.

#### Serpentinitized harzburgites (Samples 4R-1, 19–21 cm; 5R-2, 92–94 cm; 5R-2, 142–145 cm; 7R-1, 17–18 cm)

The opx porphyroclasts may exceed 1 cm in size. They are weakly elongated in the foliation of the samples (Pl. 1, Fig. 1), and locally recrystallized in polygonal grains (< 0.5 mm). The opx is partly altered to bastite, tremolite-actinolite, and talc. Cpx occurs as thin exsolution lamellae parallel to (100), as millimeter-sized porphyroclasts, or as small recrystallized grains (< 0.5 mm). The cpx is quite resistant to alteration to tremolite, and not serpentinitized. Reddish-brown Cr-spinels, 1–3 mm long and with their margins systematically transformed to black magnetite, are elongated in the foliation plane and often segmented. Other small and vermicular spinel crystals are associated with lobate extremities of the large opx porphyroclasts (Pl. 1, fig. 3). As in the dunite, the olivine porphyroclasts (up to 2 mm in size) are recrystallized into polygonal grains (0.2–0.4 mm in size) and affected by the typical mesh-like serpentinitization including small grains of magnetite.

#### Serpentinitized lherzolites (Samples 5R-1, 2–6 cm; 6R-1, 40–41 cm; 6R-1, 49–51 cm)

These samples include centimeter-sized clusters of cpx and opx crystals, associated with vermicular spinels. The modal ratio of cpx ranges from 5% to 14.5% (Sample 5R-1, 2–6 cm), or 6.5%–19% in the protoliths (before serpentinitization), if a volume increase of 30% during serpentinitization is taken into account. Apart from the large size of the pyroxene-rich clusters, the textural characteristics of the lherzolitic samples are similar to those described for the harzburgitic samples. In

**Table 1. Modal analyses of the nine selected samples. Primary phases are olivine (ol), orthopyroxene (opx), clinopyroxene (cpx), and spinel (spin). Secondary phases are serpentine (serp), including bastite, talc and magnetite, and amphibole (amph). The numbers in parentheses indicate the "dry" modal percentage of the four primary phases, calculated following the conventions indicated in the text (not taking into account the volume increase during serpentinitization). The modal proportion of clinopyroxene, taking this volume increase into account, are shown in double parentheses. Rock types are: H = harzburgite; L = lherzolite; D = dunite; and W = olivine websterite.**

Sample	Ol	Opx	Cpx	Spin	Serp	Amph	Rock type
4R-1 (#3) 19–21	12.4 (82.9)	5.2 (12.4)	3.0 (4.0) ((4.9))	0.6 (0.6)	75.4	3.3	H
5R-1 (#1) 2–6	15.4 (68.7)	6.2 (15.3)	12.2 (14.5) ((16.9))	1.4 (1.4)	57.1	7.6	L
5R-2 (#12) 92–94	13.0 (79.6)	1.1 (14.0)	3.0 (4.9) ((6.0))	1.4 (1.4)	74.9	6.5	H-L
5R-2 (#19) 142–145	19.4 (69.6)	11.8 (19.6)	1.0 (3.0) ((3.5))	7.7 (7.7)	57.9	2.0	H
6R-1 (#6) 40–41	30.8 (76.0)	4.6 (14.4)	7.6 (8.3) ((9.6))	1.2 (1.2)	53.5	2.2	L
6R-1 (#8) 49–51	27.1 (79.4)	5.4 (12.3)	6.1 (7.5) ((8.8))	0.8 (0.8)	59.2	1.4	L
7R-1 (#2) 7–10	22.1 (99.4)		0.6 (0.6) ((0.7))	tr	77.3	—	D
7R-1 (#3) 17–18	12.7 (77.5)	4.9 (17.0)	2.7 (4.8) ((5.8))	0.7 (0.7)	71.9	7.0	H-L
9R-1 (#3) 19–20	10.6 (12.0)	33.2 (42.2)	38.1 (45.7) ((46.0))	0.1 (0.1)	2.9	15.	W

Sample 6R-1, 49–51 cm, the opx and cpx porphyroclasts in the clusters are kinked and partly recrystallized into aggregates of opx, cpx, and olivine polygonal grains (Pl. 1, Fig. 2). This feature may indicate that these clusters experienced partial melting during their high-temperature deformational history. Besides, the clusters of opx, cpx, and vermicular spinel point to an exsolution of this assemblage from a former high-temperature opx.

#### Olivine websterite (Sample 9R-1, 19–20 cm)

The unique sample of websterite in our collection is nearly devoid of serpentine (2.3%, and about 15% secondary amphibole). This fresh rock (Pl. 1, Fig. 4) is made of a roughly equal number of cpx and opx porphyroclasts (Table 1), which are kinked and recrystallized into small polygonal neoblasts. Small and interstitial olivine crystals, plastically deformed and displaying subgrain boundaries, cement the pyroxene phases, along with rare euhedral Cr-spinel grains. It is clear that this websterite was involved in the high-temperature plastic deformation affecting the surrounding peridotites.

Bands of analogous plagioclase-free olivine websterite were described in residual peridotite samples from the Kane and Islas Orcadas Fracture Zones, and were interpreted as trapped melts crystallized "in situ" (Dick et al., 1984). Table 2 gives the modal compositions of these olivine websterite samples, compared with our olivine websterite Sample 9R-1, #3, which appears to have the highest content in pyroxenes and Di/En ratio, and is rather close to the Kane F.Z. sample composition.

### ELECTRON MICROPROBE ANALYSES OF THE PRIMARY PHASES

#### Analytical conditions

The microprobe analyses presented in Table 2 were performed by E. Berger, M. C. Forette, and G. Frot, using the automatized CAMEBAX microprobe of the Ecole des Mines de Paris. Each value quoted in Table 2 was obtained by the double measurement method proposed by Marion and Vanier (1983). Analytical conditions were as follows:

#### Silicates:

Program 320. H.T. = 20 kv. I = 16 nA. Four spectrometers used (PET, LIF, TAP, TAP). Counting time (with one unit = 10 s): For Na, Mg, Si, Ti, Cr, and Mn, 4 units. For Al, Ca, and Fe, 6 units. For Ni, 12 units.

#### Spinels:

Program 302. H.T. = 20 kv. I = 14 nA, except for Mn and Si for which I = 42 nA. Four spectrometers used (LIF, LIF, PET, TAP). Counting time: For Al, 1 unit. For Cr and Mg, 2

units. For V, Fe, Zn, Ni, and Ti, 6 units. For Mn and Si: 12 units.

Additional microprobe analyses on two highly deformed harzburgites (samples 4R-1, 27–30 cm, and 8R-1, 2–4 cm) were performed in Brest using the automatized CAMEBAX microprobe, equipped with four spectrometers. This additional set of data concerns specifically the interstitial cpx crystals found in the shear bands of the most strongly deformed samples (see Cannat et al., this volume).

### RESULTS

The analytical data for the nine selected samples are presented in Table 3, along with the cationic formulas of the mineral phases and some remarkable ratios or parameters. Table 4 is a summary of the values of these chemical parameters for the four primary phases in each of the nine samples. Table 5 gives overall averages of the chemical parameters for the same phases (ol, opx, cpx, and sp) in the eight serpentinized peridotites and in the olivine websterite.

#### Olivine

The olivine composition is fairly constant in the nine selected samples (Tables 2 and 3; Fig. 3). There are no significant core/rim variations. In the olivine websterite, Fo (91.03%) and NiO (0.41%) are slightly higher than in the serpentinized dunite, harzburgites, and lherzolites (Fo: 90.4%–90.95%, NiO: 0.37%–0.40%). There are no systematic compositional variations between the olivine from these last three petrographic facies (Fig. 3).

#### Orthopyroxene

There are no systematic compositional variations between the opx from the four petrographic facies (serpentinized dunite, harzburgite, lherzolite, and websterite; Tables 3 and 4; Fig. 4). The Wo contents range from 1.73% to 2.92% (2.21% in the websterite). The En contents range from 87.07% to 88.85% (88.59% in the websterite). The Al<sub>2</sub>O<sub>3</sub> contents range from 3.33% to 5.67% (4.17% in the websterite). There is a good positive correlation between the Wo and Al<sub>2</sub>O<sub>3</sub> contents, and the compositional variations between two grains of the same sample often exceed the variations observed between opx crystals from distinct petrographic facies. The rims of some porphyroclasts are slightly depleted in Al, Cr, and Wo contents, but this core/rim variation is not observed in all samples. The small polygonal grains recrystallized during the plastic deformation of the samples are devoid of cpx exsolution lamellae. They show slightly lower Al and Wo contents (and higher En contents) than the original porphyroclasts.

#### Clinopyroxene

As for the opx, there are no systematic compositional variations between the cpx of the four petrographic facies (Tables 3 and 4). The Al<sub>2</sub>O<sub>3</sub> contents range from 4.25% to 6.07% (5.39%–5.73% in the websterite). The TiO<sub>2</sub> and Na<sub>2</sub>O contents are usually low. TiO<sub>2</sub> ranges from 0.11% to 0.25% (0.11%–0.13% in the websterite), and Na<sub>2</sub>O ranges from 0.11% to 0.22% (0.15%–0.16% in the websterite). There is no systematic correlation between the Al<sub>2</sub>O<sub>3</sub>, TiO<sub>2</sub>, Na<sub>2</sub>O, and CaO contents of the cpx. In one harzburgite sample cpx porphyroclast yields a Na<sub>2</sub>O content of 0.39% (Table 3). This porphyroclast also yields the lowest Al<sub>2</sub>O<sub>3</sub> content. The rims of most cpx porphyroclasts are distinctly depleted in Al and Cr, while Mg and Ca tend to increase. The small polygonal neoblasts recrystallized during the plastic deformation also show lower Al and Cr contents than the original porphyroclasts.

**Table 2. Modal analyses of two olivine websterites collected in the North Atlantic Ocean (after Dick et al., 1984), and comparison with the modal composition of Site 670 olivine websterite, Sample 9R-1, 19–20 cm (#3).**

Locality	Olivine	Enstatite	Diopside	Spinel
Kane Fracture Zone AII 96-1-3	20.8	43.1	34.3	1.8
Islas Orcadas Fracture Zone 1011/76-60-52	28.8	53.2	17.3	0.7
Hole ODP 670A 9R-1 (#3) 19–20 cm	12.0	42.2	45.7	0.1

**Table 3. Microprobe analyses of the primary phases of the nine selected samples. Each section corresponds to one sample. The analyzed phases are: olivine (OL), orthopyroxene (OPX), clinopyroxene (CPX), spinel (SP), and one amphibole inclusion (Amph). (C) = core; (B) = margin. Inclusions or exsolution lamellae are distinguished by the symbol of the host-mineral following the symbol of the phase analyzed. FeO\* = total iron (microprobe). FeO and Fe<sub>2</sub>O<sub>3</sub> calculated assuming stoichiometry, as well as AlIV and AlVI distribution. m = 100 Mg/(Mg + Fe<sup>2+</sup> + Fe<sup>3+</sup>). M = 100 Mg/(Mg + Fe<sup>2+</sup>). Cr# = 100 Cr/(Cr + Al).**

4R-1, #32	Oll(C)	Opx1(C)	Sp1	Sp2
SiO <sub>2</sub>	41.01	55.41	0.05	0.03
Al <sub>2</sub> O <sub>3</sub>	0.01	3.86	40.52	41.54
TiO <sub>2</sub>	0.00	0.07	0.12	0.08
Cr <sub>2</sub> O <sub>3</sub>	0.00	0.90	26.38	26.20
V <sub>2</sub> O <sub>3</sub>	0.00	0.00	0.15	0.13
Fe <sub>2</sub> O <sub>3</sub>	0.00	0.00	2.88	2.36
FeO	8.95	5.83	12.33	11.77
MnO	0.12	0.15	0.18	0.17
MgO	49.39	32.66	17.02	17.50
CaO	0.08	1.25	0.00	0.00
Na <sub>2</sub> O	0.00	0.02	0.00	0.00
NiO	0.40	0.09	0.23	0.25
ZnO	0.00	0.00	0.19	0.21
Total	99.96	100.24	100.05	100.24
FeO*	8.95	5.83	14.92	13.89
Si	1.003	1.912	0.011	0.007
AlIV	0.000	0.088	0.000	0.000
AlVI	0.000	0.069	10.692	10.872
Ti	0.000	0.002	0.020	0.013
Cr	0.000	0.025	4.671	4.602
V	0.000	0.000	0.027	0.023
Fe <sup>3+</sup>	0.000	0.000	0.485	0.394
Fe <sup>2+</sup>	0.182	0.168	2.304	2.181
Mn	0.002	0.004	0.034	0.032
Mg	1.799	1.678	5.683	5.796
Ca	0.002	0.046	0.000	0.000
Na	0.000	0.001	0.000	0.000
Ni	0.008	0.002	0.041	0.045
Zn	0.000	0.000	0.031	0.034
Total	2.996	3.995	23.999	23.999
m	90.8	90.89	67.07	69.23
M	90.8	90.89	71.15	72.65
Wo		2.44		
En		88.68		
Fs		8.88		
Cr#			30.4	29.74

5R-1, #1	Oll(C)	Opx1(C)	Opx1(B)	Cpx1(C)	Cpx1(B)	Sp1(C)	Sp1(B)
SiO <sub>2</sub>	40.83	55.51	54.72	50.64	50.93	0.07	0.07
Al <sub>2</sub> O <sub>3</sub>	0.01	3.85	4.17	5.88	5.64	50.18	49.85
TiO <sub>2</sub>	0.00	0.05	0.06	0.13	0.25	0.06	0.03
Cr <sub>2</sub> O <sub>3</sub>	0.00	0.64	0.48	1.30	1.15	17.07	17.36
V <sub>2</sub> O <sub>3</sub>	0.00	0.00	0.00	0.00	0.00	0.11	0.08
Fe <sub>2</sub> O <sub>3</sub>	0.00	0.00	0.21	0.49	0.32	1.67	1.60
FeO	9.14	5.97	5.83	2.55	2.73	11.82	12.12
MnO	0.19	0.16	0.15	0.11	0.11	0.15	0.14
MgO	49.20	32.36	32.54	16.56	16.85	18.34	18.09
CaO	0.05	1.33	1.14	21.67	21.56	0.00	0.00
Na <sub>2</sub> O	0.00	0.01	0.01	0.15	0.13	0.00	0.00
NiO	0.38	0.09	0.09	0.08	0.07	0.27	0.26
ZnO	0.00	0.00	0.00	0.00	0.00	0.23	0.25
Total	99.80	99.97	99.40	99.56	99.74	99.97	99.85
FeO*	9.14	5.97	6.02	2.99	3.02	13.32	13.56
Si	1.002	1.920	1.904	1.850	1.856	0.015	0.015
AlIV	0.000	0.080	0.096	0.150	0.144	0.000	0.000
AlVI	0.000	0.077	0.075	0.103	0.098	12.692	12.652
Ti	0.000	0.001	0.002	0.004	0.007	0.010	0.005
Cr	0.000	0.017	0.013	0.037	0.033	2.897	2.957
V	0.000	0.000	0.000	0.000	0.000	0.019	0.014
Fe <sup>3+</sup>	0.000	0.000	0.005	0.013	0.009	0.270	0.259
Fe <sup>2+</sup>	0.187	0.172	0.169	0.078	0.083	2.117	2.179
Mn	0.004	0.005	0.004	0.003	0.003	0.027	0.026
Mg	1.797	1.667	1.686	0.901	0.914	5.870	5.810
Ca	0.001	0.049	0.043	0.848	0.842	0.000	0.000
Na	0.000	0.001	0.001	0.011	0.009	0.000	0.000
Ni	0.007	0.003	0.003	0.002	0.002	0.047	0.045
Zn	0.000	0.000	0.000	0.000	0.000	0.036	0.040
Total	2.998	3.992	4.001	4.000	4.000	24.000	24.002

Table 3 (continued).

5R-1, #1	O11(C)	Opx1(C)	Opx1(B)	Cpx1(C)	Cpx1(B)	Sp1(C)	Sp1(B)
m	90.57	90.64	90.64	90.81	90.84	71.09	70.44
M	90.57	90.64	90.88	92.02	91.66	73.49	72.72
Wo		2.61	2.23	46.07	45.53		
En		88.26	88.57	48.97	49.49		
Fs		9.14	9.20	4.96	4.98		
Cr#						18.58	18.94

5R1, #12	O11(C)	O12(C)	Cpx1(C)	Sp1(C)	Sp1(B)	Sp2(C)
SiO <sub>2</sub>	40.95	41.02	50.80	0.00	0.00	0.09
Al <sub>2</sub> O <sub>3</sub>	0.02	0.00	5.94	47.56	47.91	47.42
TiO <sub>2</sub>	0.00	0.00	0.14	0.06	0.06	0.05
Cr <sub>2</sub> O <sub>3</sub>	0.00	0.00	1.13	19.45	19.15	19.76
V <sub>2</sub> O <sub>3</sub>	0.00	0.00	0.00	0.10	0.12	0.10
Fe <sub>2</sub> O <sub>3</sub>	0.00	0.00	0.93	2.87	2.55	2.54
FeO	8.99	9.00	2.22	10.45	11.39	11.01
MnO	0.09	0.24	0.11	0.15	0.14	0.15
MgO	49.54	49.53	16.84	18.81	18.42	18.55
CaO	0.05	0.04	21.66	0.00	0.00	0.00
Na <sub>2</sub> O	0.00	0.00	0.16	0.00	0.00	0.00
NiO	0.40	0.37	0.08	0.26	0.30	0.25
ZnO	0.00	0.00	0.00	0.13	0.30	0.12
Total	100.04	100.20	100.01	99.84	100.34	100.04
FeO*	8.99	9.00	3.061	3.031	3.69	13.30
Si	1.001	1.002	1.846	0.000	0.000	0.020
AlIV	0.000	0.000	0.154	0.000	0.000	0.000
AlVI	0.001	0.000	0.100	12.128	12.183	12.094
Ti	0.000	0.000	0.004	0.010	0.010	0.008
Cr	0.000	0.000	0.032	3.328	3.268	3.382
V	0.000	0.000	0.000	0.017	0.021	0.017
Fe <sup>3+</sup>	0.000	0.000	0.025	0.466	0.413	0.413
Fe <sup>2+</sup>	0.183	0.183	0.067	1.888	2.052	1.989
Mn	0.002	0.005	0.003	0.027	0.026	0.027
Mg	1.803	1.801	0.911	6.070	5.928	5.987
Ca	0.001	0.001	0.843	0.000	0.000	0.000
Na	0.000	0.000	0.011	0.000	0.000	0.000
Ni	0.008	0.007	0.002	0.045	0.052	0.044
Zn	0.000	0.000	0.000	0.021	0.048	0.019
Total	2.999	2.999	3.998	24.000	24.001	24.000
m	90.78	90.77	90.81	72.05	70.62	71.36
M	90.78	90.77	93.13	76.27	74.28	75.06
Wo				45.63		
En				49.34		
Fs				5.03		
CR#				21.53	21.15	21.85

5R2, #19	O11	Opx1(C)	Opx2	Cpx1	Sp1(C)	Sp1(B)
SiO <sub>2</sub>	41.06	54.96	55.14	52.12	0.04	0.08
Al <sub>2</sub> O <sub>3</sub>	0.02	4.42	3.72	4.25	42.50	44.93
TiO <sub>2</sub>	0.00	0.05	0.06	0.20	0.08	0.09
Cr <sub>2</sub> O <sub>3</sub>	0.00	0.88	0.64	0.98	24.95	22.50
V <sub>2</sub> O <sub>3</sub>	0.00	0.00	0.00	0.00	0.05	0.10
Fe <sub>2</sub> O <sub>3</sub>	0.00	0.00	0.00	0.38	3.11	2.69
FeO	8.77	5.94	6.13	2.54	10.74	10.28
MnO	0.10	0.15	0.14	0.18	0.15	0.16
MgO	49.45	31.95	32.36	16.98	18.23	18.75
CaO	0.14	1.49	1.39	21.60	0.00	0.00
Na <sub>2</sub> O	0.00	0.04	0.04	0.39	0.00	0.00
NiO	0.39	0.09	0.09	0.08	0.28	0.30
ZnO	0.00	0.00	0.00	0.00	0.14	0.14
Total	99.93	99.97	99.71	99.70	100.27	100.02
FeO*	8.77	5.94	6.13	2.89	13.54	12.70
Si	1.004	1.904	1.916	1.898	0.009	0.017
AlIV	0.000	0.096	0.084	0.102	0.000	0.000
AlVI	0.001	0.084	0.068	0.080	11.038	11.551
Ti	0.000	0.001	0.002	0.005	0.013	0.015
Cr	0.000	0.024	0.018	0.028	4.348	3.882
V	0.000	0.000	0.000	0.000	0.000	0.017
Fe <sup>3+</sup>	0.000	0.000	0.000	0.010	0.515	0.440
Fe <sup>2+</sup>	0.179	0.171	0.177	0.077	1.976	1.872
Mn	0.002	0.004	0.004	0.006	0.028	0.030
Mg	1.800	1.648	1.674	0.921	5.992	6.100
Ca	0.004	0.055	0.052	0.843	0.000	0.000
Na	0.000	0.003	0.003	0.027	0.000	0.000
Ni	0.008	0.003	0.003	0.002	0.050	0.053
Zn	0.000	0.000	0.000	0.000	0.023	0.023
Total	2.998	3.993	4.001	3.9992	4.001	24.000

Table 3 (continued).

5R2, #19	O11	Opx1(C)	Opx2	Cpx1	Sp1(C)	Sp1(B)	
m	90.95	90.59	90.43	91.35	70.63	72.51	
M	90.95	90.59	90.43	92.27	75.19	76.51	
Wo		2.95	2.72	45.50			
En		87.88	87.94	49.75			
Fs		9.17	9.35	4.75			
Cr#					28.25	25.15	

6R1, #6	O1	Opx1	Opx2	Cpx1	Cpx2	Sp1(C)	Sp2
SiO <sub>2</sub>	41.24	56.22	55.06	52.20	51.00	0.10	0.09
Al <sub>2</sub> O <sub>3</sub>	0.00	3.33	4.41	4.62	5.75	47.61	50.15
TiO <sub>2</sub>	0.00	0.05	0.10	0.25	0.12	0.07	0.15
Cr <sub>2</sub> O <sub>3</sub>	0.00	0.39	0.76	0.85	1.17	19.16	17.32
V <sub>2</sub> O <sub>3</sub>	0.00	0.00	0.00	0.00	0.00	0.08	0.08
Fe <sub>2</sub> O <sub>3</sub>	0.00	0.00	0.00	0.00	0.00	2.90	1.63
FeO	8.82	6.10	6.15	3.00	2.941	0.54	11.98
MnO	0.15	0.15	0.04	0.01	0.11	0.13	0.15
MgO	49.40	32.98	32.32	17.12	16.36	18.86	18.22
CaO	0.02	0.89	0.95	21.83	21.98	0.00	0.00
Na <sub>2</sub> O	0.00	0.00	0.04	0.11	0.11	0.00	0.00
NiO	0.40	0.08	0.10	0.08	0.06	0.29	0.37
ZnO	0.00	0.00	0.00	0.00	0.00	0.14	0.10
Total	100.03	100.19	99.93	100.07	99.60	99.88	100.24
FeO*	8.82	6.10	6.15	3.00	2.94	13.15	13.44
Si	1.007	1.937	1.906	1.893	1.862	0.022	0.019
AlIV	0.000	0.063	0.094	0.107	0.138	0.000	0.000
AlVI	0.000	0.072	0.085	0.090	0.109	12.128	12.670
Ti	0.000	0.001	0.003	0.007	0.003	0.011	0.024
Cr	0.000	0.011	0.021	0.024	0.034	3.275	2.936
V	0.000	0.000	0.000	0.000	0.000	0.014	0.014
Fe <sup>3+</sup>	0.000	0.000	0.000	0.000	0.000	0.472	0.262
Fe <sup>2+</sup>	0.179	0.175	0.177	0.091	0.089	1.901	2.143
Mn	0.003	0.004	0.001	0.000	0.003	0.024	0.027
Mg	1.796	1.691	1.665	0.924	0.889	6.080	5.825
Ca	0.001	0.033	0.035	0.848	0.860	0.000	0.000
Na	0.000	0.000	0.003	0.008	0.008	0.000	0.000
Ni	0.008	0.002	0.003	0.002	0.002	0.050	0.064
Zn	0.000	0.000	0.000	0.000	0.000	0.022	0.016
Total	2.994	3.989	3.993	3.994	3.997	23.999	24.000
m	90.93	90.61	90.38	91.02	90.89	71.92	70.77
M	90.93	90.61	90.38	91.02	90.89	76.17	73.10
Wo		1.73	1.87	45.50	46.74		
En		89.03	88.66	49.63	48.38		
Fs		9.24	9.47	4.88	4.88		
Cr#						21.26	18.81

6R1, #8	O11(C)	Opx1(C)	Opx3(CP)	Cpx1(C)	Cpx3(C)	Sp1(C)	Sp2(C)
SiO <sub>2</sub>	40.86	55.00	54.07	50.60	50.75	0.03	0.04
Al <sub>2</sub> O <sub>3</sub>	0.01	4.19	5.67	6.07	6.04	46.88	49.13
TiO <sub>2</sub>	0.00	0.07	0.04	0.16	0.12	0.30	0.03
Cr <sub>2</sub> O <sub>3</sub>	0.00	0.46	1.03	1.26	1.26	20.18	18.42
V <sub>2</sub> O <sub>3</sub>	0.00	0.00	0.00	0.00	0.00	0.09	0.09
Fe <sub>2</sub> O <sub>3</sub>	0.02	0.03	0.00	1.29	1.13	2.36	1.78
FeO	9.06	6.29	6.30	2.13	2.16	11.37	11.11
MnO	0.16	0.17	0.14	0.11	0.08	0.14	0.14
MgO	49.51	32.50	31.97	17.34	16.77	18.37	18.59
CaO	0.03	1.09	0.832	0.81	21.55	0.00	0.00
Na <sub>2</sub> O	0.00	0.01	0.03	0.17	0.22	0.00	0.00
NiO	0.38	0.09	0.09	0.10	0.08	0.30	0.30
ZnO	0.00	0.00	0.00	0.00	0.00	0.14	0.20
Total	100.03	99.90	100.17	100.04	100.16	100.16	99.83
FeO*	9.07	6.32	6.30	3.29	3.18	13.49	12.71
Si	1.000	1.906	1.871	1.836	1.842	0.007	0.009
AlIV	0.000	0.094	0.129	0.164	0.158	0.000	0.000
AlVI	0.000	0.077	0.102	0.096	0.100	11.983	12.469
Ti	0.000	0.002	0.001	0.004	0.003	0.049	0.005
Cr	0.000	0.013	0.028	0.036	0.036	3.461	3.137
V	0.000	0.000	0.000	0.000	0.000	0.016	0.016
Fe <sup>3+</sup>	0.000	0.001	0.000	0.035	0.031	0.385	0.288
Fe <sup>2+</sup>	0.185	0.182	0.182	0.064	0.065	2.058	1.997
Mn	0.003	0.005	0.004	0.003	0.002	0.026	0.026
Mg	1.804	1.677	1.647	0.937	0.906	5.942	5.971
Ca	0.001	0.040	0.031	0.809	0.838	0.000	0.000
Na	0.000	0.001	0.002	0.012	0.015	0.000	0.000
Ni	0.007	0.003	0.003	0.003	0.002	0.052	0.052
Zn	0.000	0.000	0.000	0.000	0.000	0.022	0.032
Total	3.000	4.001	4.000	3.999	3.998	24.001	24.002

**Table 3 (continued).**

6R1, #8	O11(C)	Opx1(C)	Opx3(CP)	Cpx1(C)	Cpx3(C)	Sp1(C)	Sp2(C)
m	90.69	90.15	90.04	90.43	90.41	70.86	72.32
M	90.69	90.20	90.04	93.59	93.29	74.27	74.93
Wo		2.13	1.654	3.814	5.51		
En		88.24	88.55	50.78	49.25		
Fs		9.63	9.79	5.41	5.24		
Cr#						22.4	20.1

7R1, #2	O11(C)	Cpx2(C)	Sp1	Sp3
SiO <sub>2</sub>	40.95	50.95	0.08	0.12
Al <sub>2</sub> O <sub>3</sub>	0.03	5.63	46.40	45.97
TiO <sub>2</sub>	0.01	0.16	0.05	0.07
Cr <sub>2</sub> O <sub>3</sub>	0.00	1.25	19.77	17.40
V <sub>2</sub> O <sub>3</sub>	0.00	0.00	0.10	0.14
Fe <sub>2</sub> O <sub>3</sub>	0.00	0.64	2.42	4.99
FeO	9.30	2.32	12.37	14.22
MnO	0.15	0.11	0.16	0.16
MgO	49.18	16.63	17.39	16.45
CaO	0.09	22.06	0.00	0.00
Na <sub>2</sub> O	0.00	0.15	0.00	0.00
NiO	0.38	0.08	0.28	0.27
ZnO	0.00	0.00	0.19	0.35
Total	100.09	99.98	99.21	100.14
FeO*	9.30	2.90	14.55	18.71
Si	1.002	1.854	0.018	0.026
AlIV	0.000	0.146	0.000	0.000
AlVI	0.001	0.095	12.029	11.930
Ti	0.000	0.004	0.008	0.012
Cr	0.000	0.036	3.439	3.030
V	0.000	0.000	0.018	0.025
Fe <sup>3+</sup>	0.000	0.017	0.400	0.825
Fe <sup>2+</sup>	0.190	0.070	2.272	2.615
Mn	0.003	0.003	0.030	0.030
Mg	1.792	0.901	5.705	5.403
Ca	0.002	0.860	0.000	0.000
Na	0.000	0.011	0.000	0.000
Ni	0.007	0.002	0.050	0.048
Zn	0.000	0.000	0.031	0.057
Total	2.997	3.999	24.000	24.001
m	90.4	91.18	68.10	61.09
M	90.4	92.78	71.51	67.38
Wo		46.49		
En		48.74		
Fs		4.77		
Cr#			22.23	20.25

7R1, #3	O11(C)	Opx1(C)	Opx1(B)	Cpx	Amph(OP)	Sp1(C)	Sp1(B)
SiO <sub>2</sub>	41.08	54.22	54.99	52.19	52.45	0.03	0.03
Al <sub>2</sub> O <sub>3</sub>	0.00	4.89	4.39	4.29	5.45	46.84	46.42
TiO <sub>2</sub>	0.00	0.06	0.07	0.15	0.15	0.08	0.07
Cr <sub>2</sub> O <sub>3</sub>	0.00	0.87	0.79	0.84	0.962	0.652	0.51
V <sub>2</sub> O <sub>3</sub>	0.00	0.00	0.00	0.00	0.00	0.09	0.13
Fe <sub>2</sub> O <sub>3</sub>	0.00	0.11	0.00	0.42	0.00	2.63	2.85
FeO	9.07	6.00	5.94	2.59	3.95	10.56	10.95
MnO	0.16	0.15	0.15	0.14	0.11	0.15	0.16
MgO	49.22	31.99	32.28	17.31	22.07	18.74	18.40
CaO	0.12	1.29	1.18	22.01	13.24	0.00	0.00
Na <sub>2</sub> O	0.00	0.01	0.01	0.16	0.13	0.00	0.00
NiO	0.39	0.11	0.10	0.07	0.09	0.30	0.28
ZnO	0.00	0.00	0.00	0.00	0.00	0.11	0.13
Total	100.04	99.70	99.90	100.17	98.60	100.18	99.93
FeO*	9.07	6.10	5.94	2.96	3.95	12.93	13.51
Si	1.005	1.885	1.904	1.892	7.245	0.007	0.007
AlIV	0.000	0.115	0.096	0.108	0.755	0.000	0.000
AlVI	0.000	0.085	0.083	0.075	0.131	11.948	11.905
Ti	0.000	0.002	0.002	0.004	0.016	0.013	0.011
Cr	0.000	0.024	0.022	0.024	0.105	3.535	3.530
V	0.000	0.000	0.000	0.000	0.000	0.016	0.023
Fe <sup>3+</sup>	0.000	0.003	0.000	0.011	0.000	0.428	0.465
Fe <sup>2+</sup>	0.185	0.174	0.171	0.078	0.455	1.908	1.989
Mn	0.003	0.004	0.004	0.004	0.013	0.027	0.029
Mg	1.792	1.656	1.664	0.934	4.539	6.049	5.972
Ca	0.003	0.048	0.044	0.855	1.960	0.000	0.000
Na	0.000	0.001	0.001	0.011	0.035	0.000	0.000
Ni	0.008	0.003	0.003	0.002	0.010	0.052	0.049
Zn	0.000	0.000	0.000	0.000	0.000	0.018	0.021
Total	2.996	4.000	3.994	3.998	15.264	24.001	24.001

Table 3 (continued).

7R1, #3	O11(C)	Opx1(C)	Opx1(B)	Cpx	Amph(OP)	Sp1(C)	Sp1(B)
m	90.63	90.33	90.67	91.29	90.88	72.13	70.87
M	90.63	90.48	90.67	92.28	90.88	76.02	75.01
Wo		2.55	2.33	45.48			
En		88.03	88.53	49.75			
Fs		9.42	9.14	4.77			
Cr#						22.83	22.87
9R1, #3	O11	Opx3(C)	Opx(B)	Cpx1(C)	Cpx	Sp4	Sp1
SiO <sub>2</sub>	41.00	55.35	54.96	51.32	50.84	0.07	0.11
Al <sub>2</sub> O <sub>3</sub>	0.03	4.17	4.28	5.39	5.73	53.00	53.60
TiO <sub>2</sub>	0.00	0.03	0.03	0.13	0.11	0.02	0.02
Cr <sub>2</sub> O <sub>3</sub>	0.00	0.46	0.45	0.87	0.86	13.59	13.12
V <sub>2</sub> O <sub>3</sub>	0.00	0.00	0.00	0.00	0.00	0.16	0.08
Fe <sub>2</sub> O <sub>3</sub>	0.00	0.00	0.14	0.86	1.15	1.18	1.11
FeO	8.73	5.85	5.83	2.19	1.91	12.18	12.37
MnO	0.14	0.17	0.13	0.10	0.12	0.18	0.15
MgO	49.74	32.61	32.63	17.41	16.66	18.47	18.46
CaO	0.02	1.13	1.16	21.39	22.19	0.00	0.00
Na <sub>2</sub> O	0.00	0.04	0.03	0.16	0.15	0.00	0.00
NiO	0.41	0.09	0.09	0.06	0.09	0.30	0.34
ZnO	0.00	0.00	0.00	0.00	0.00	0.56	0.53
Total	100.07	99.90	99.73	99.88	99.81	99.71	99.89
FeO*	8.73	5.85	5.96	2.97	2.94	13.25	13.37
Si	1.001	1.914	1.905	1.863	1.851	0.015	0.023
AlIV	0.000	0.086	0.095	0.137	0.149	0.000	0.000
AlVI	0.001	0.083	0.080	0.093	0.097	13.286	13.390
Ti	0.000	0.001	0.001	0.004	0.003	0.003	0.003
Cr	0.000	0.013	0.012	0.025	0.025	2.286	2.199
V	0.000	0.000	0.000	0.000	0.000	0.027	0.014
Fe <sup>3+</sup>	0.000	0.000	0.004	0.024	0.031	0.189	0.177
Fe <sup>2+</sup>	0.178	0.169	0.168	0.066	0.058	2.163	2.188
Mn	0.003	0.005	0.004	0.003	0.004	0.032	0.027
Mg	1.808	1.679	1.684	0.941	0.903	5.859	5.836
Ca	0.001	0.042	0.043	0.832	0.866	0.000	0.000
Na	0.000	0.003	0.002	0.011	0.011	0.000	0.000
Ni	0.008	0.002	0.003	0.002	0.003	0.051	0.058
Zn	0.000	0.000	0.000	0.000	0.000	0.088	0.083
Total	3.000	3.997	4.001	4.001	4.001	23.999	23.998
m	91.03	90.85	90.72	91.26	91.01	71.35	71.16
M	91.03	90.85	90.92	93.43	93.95	73.03	72.73
Wo		2.21	2.27	44.63	46.56		
En		88.84	88.65	50.53	48.62		
Fs		8.94	9.09	4.84	4.82		
Cr#						14.68	14.10

Table 4. Summary of the chemical compositions of selected primary phases (cores only) in the nine studied samples.

	Olivine		Orthopyroxene			Clinopyroxene			Spinel	
	Fo	NiO	En	Wo	Al <sub>2</sub> O <sub>3</sub>	Al <sub>2</sub> O <sub>3</sub>	TiO <sub>2</sub>	Na <sub>2</sub> O	Al <sub>2</sub> O <sub>3</sub>	Cr <sub>2</sub> O <sub>3</sub>
7R-1, #2, (7-10 cm) Dunite	90.4	0.38				5.63	0.16	0.15	46.50	19.77
									45.97	17.40
									40.52	26.38
									41.54	26.20
						4.25	0.20	0.39	42.50	24.95
4R-1, #3, (19-21 cm) Harzburgite	90.8	0.40	88.49	2.42	3.86	4.29	0.15	0.16	46.84	20.65
5R-2, #19, (142-145 cm) Harzburgite	90.95	0.39	87.74	2.92	4.42	5.94	0.14	0.16	47.56	19.45
			87.77	2.72	3.72				47.42	19.76
7R-1, #3, (17-18 cm) Harzburgite	90.63	0.39	87.98	2.55	4.89	5.88	0.13	0.15	50.18	17.07
5R-2, #12, (92-94 cm) Harzburgite	90.78	0.40				4.62	0.25	0.11	47.61	19.16
	90.77	0.37				5.75	0.12	0.11	50.15	17.32
5R-1, #1, (2-6 cm) Lherzolite	90.57	0.38	88.05	2.58	3.85	6.07	0.16	0.17	46.88	20.18
6R-1, #6, (40-41 cm) Lherzolite	90.93	0.40	88.85	1.73	3.33	6.04	0.12	0.22	49.13	18.42
			88.65	1.86	4.41					
6R-1, #8, (49-51 cm) Lherzolite	90.69	0.38	87.07	2.10	4.19					
			88.35	1.66	5.67					
9R-1, #3, (19-20 cm) Websterite	91.03	0.41	88.59	2.21	4.17	5.39	0.13	0.16	53.00	13.59
						5.73	0.11	0.15	53.60	13.12

**Table 5. Average values of some classical chemical parameters in the four primary mineral phases of Site 670 peridotites (eight samples) and of the olivine websterite (one sample).**

	Peridotites (8 samples)			Average Sp	Olivine websterite (1 sample)			
	Average Ol	Average Opx	Average Cpx		Ol	Opx	Cpx	Sp
CaO (wt%)		1.17				1.13		
Al <sub>2</sub> O <sub>3</sub> (wt%)		4.26	5.41	46.4		4.17	5.56	53.50
Cr <sub>2</sub> O <sub>3</sub> (wt%)		0.71	1.12	20.5		0.46	0.87	13.28
TiO <sub>2</sub> (wt%)		0.06	0.17	0.08		0.03	0.12	0.02
NiO (wt%)	0.39			0.28	0.41			0.32
Mg #9	0.79	0.59	0.8	73.6	93.7	91.3	90.9	72.9
Cr #				22.9				14.4
Wo		2.3	45.6			2.2	46.3	
En		88.4	49.4			88.8	50.3	
Fs		9.3	5.0			9.0	3.4	
Na <sub>2</sub> O (wt%)		0.02	0.18			0.04	0.16	

In the cationic formulas presented in Table 3, the distribution of Fe<sup>3+</sup> and Fe<sup>2+</sup> cations from stoichiometry is somewhat variable, since the Fe<sup>3+</sup>/Fe<sup>3+</sup> + Fe<sup>2+</sup> ratio ranges from zero to values as high as 0.35. Most of the analyzed cpx however have ratios clustered between 0.11 and 0.19, with a Fe<sup>3+</sup> content close to the Na<sup>+</sup> content in the cationic formula. The few Fe<sup>3+</sup>-rich cpx are clearly those who have a small deficit in Si<sup>4+</sup> in their formula: this may be an analytical artifact, and we reach here the limits of probe analyses accuracy.

In the most strongly deformed harzburgites of our collection, very small (<0.1 mm) interstitial cpx were found in lenses oblique on the foliation and parallel to the shear plane of the sample (see Cannat et al., this volume). This disposition is similar to that of feldspathic lenses in the Lanzo (Boudier and Nicolas, 1972) or Trinity (Le Sueur et al., 1984) lherzolites, where it is attributed to feldspar crystallization from a melt, before the end of the plastic deformation (Boudier and Nicolas, 1972; Nicolas and Jackson, 1982). This similarity suggests that the small interstitial cpx in the Site 670 peridotites may be magmatic in origin. In order to test this hypothesis, we conducted additional microprobe analyses on two highly deformed serpentized harzburgites (Samples 4R-1, 27–30 cm, and 8R-1, 2–4 cm) described by Cannat (this volume). The interstitial cpx were found to have identical compositions to the rims of the cpx porphyroclasts and recrystallized polygonal grains. Specifically, the TiO<sub>2</sub> or Na<sub>2</sub>O

contents of the interstitial cpx were in no way higher than in the other cpx crystals of the studied samples.

### Chrome spinel

By contrast with the other three primary minerals (olivine, opx, and cpx), there appears to be a definite correlation between the composition of the spinel and the petrographic facies of the analyzed sample (Tables 3 and 4; Fig. 5). In the lherzolites, the Al<sub>2</sub>O<sub>3</sub> contents range from 46.88% to 50.18% and the Cr# is 20.2 in average. The Al<sub>2</sub>O<sub>3</sub> contents are lower in the harzburgites: 40.52%–47.56%, with a Cr# of 24.6 in average. The spinels of the dunite have “harzburgitic” Al<sub>2</sub>O<sub>3</sub> contents (45.97%–46.40%) and Cr# (21.2). Lastly, the spinels of the olivine websterite are the most aluminous of all, with Al<sub>2</sub>O<sub>3</sub> contents of 53.00%–53.60%, and a Cr# in spinel as low as 14.4. The core/rim variations (slight decrease or increase of the Al<sub>2</sub>O<sub>3</sub> content) are not systematic; their study is hindered by the presence around most spinel grains of a black rim of secondary magnetite.

In the cationic formulas presented in Table 3, the distribution of Fe<sup>2+</sup> and Fe<sup>3+</sup> in spinels was done assuming stoichiometry. Here also, as in the cpx formulas, the Fe<sup>3+</sup>/Fe<sup>3+</sup> + Fe<sup>2+</sup> ratio shows some variations: from 0.08 to 0.23 in the spinels of the peridotites, and between 0.07 and 0.08 in the spinels of the olivine websterite. About two thirds of the spinels of the peridotites, however, have a fairly constant ratio comprised between 0.15 and 0.20. Taking into account that minor elements such as Ti, Cr, V, Ni, and Zn were carefully analyzed in these spinels, we think that the inferred Fe<sup>3+</sup> values in the cationic formulas are reasonably significant.

### Relationships between modal compositions and mineralogical variations

#### Dunite, harzburgites, lherzolites

In the eight selected serpentized peridotites (dunite, harzburgites, and lherzolites), the compositional variations of olivine, opx, and cpx cannot be correlated with changes in the modal composition. Specifically, the lherzolites do not have more aluminous pyroxenes, nor are they richer in incompatible elements such as Ti or Na, as could be expected if they were less residual than the harzburgites or the dunite. This supports the hypothesis that the modal heterogeneity of the samples in our collection is not due to significant variations in the degree of melting of the peridotites, but rather to the fact that these samples are approximately the same size as the cpx-opx clusters scattered through the rocks. This hypothesis is also suggested by the textural homogeneity of the three

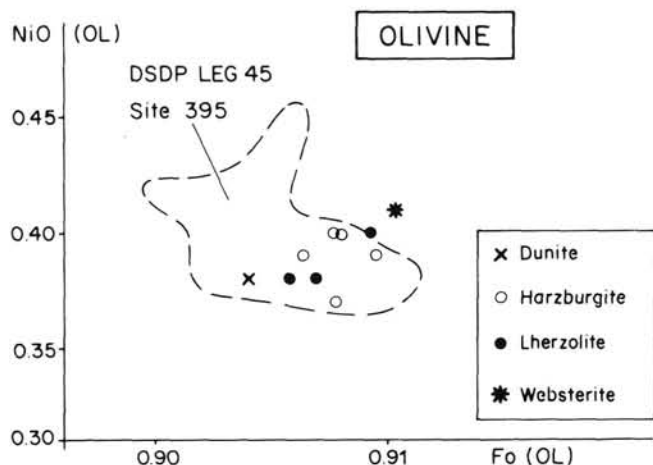


Figure 3. Diagram of the NiO content vs. Fo% of olivine in the studied samples, and comparison with Site 395 data.

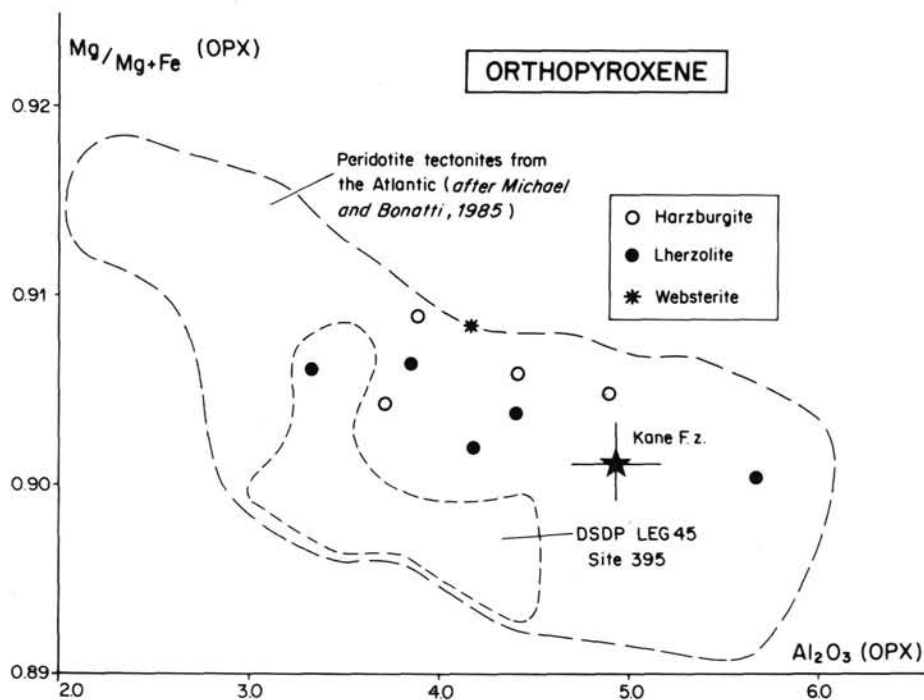


Figure 4. Diagram of the Mg/Mg + Fe ratio vs. the  $\text{Al}_2\text{O}_3$  content (wt%) in the orthopyroxenes of the studied samples, and comparison with other data from the North Atlantic area (after Michael and Bonatti, 1985).

petrographic facies. The spinel Cr# is the only parameter showing slight but systematic differences between lherzolites and harzburgites (Fig. 5): these differences could be the result of local, second order variations of the melting rate. As a consequence, we propose that a representative modal composition for the Site 670 peridotites could be an average of the modes measured for each facies, taking into account the relative proportion of each facies in our collection (29 samples, with about 60% harzburgites, 26% lherzolites, and 14% dunites). The calculated average modal composition is a cpx-poor lherzolite containing 79.6% olivine, 14% opx, 5.2% cpx, and 1.2% spinel.

#### Olivine websterite

There are no differences, in the composition of opx and cpx, between the olivine websterite sample and the peridotites. The deformed pyroxenes of the websterite are therefore in equilibrium with the pyroxenes of the surrounding peridotites, presumably residual in origin. These pyroxenes are not enriched in incompatible elements such as Al, Ti, Ca, or Na and are Mg-rich, and the olivine in this rock is especially Mg- and Ni-rich (Fig. 3). It is therefore difficult to consider this rock as the direct crystallization product of a trapped liquid extracted from the surrounding peridotite during a partial melting event. It could rather represent an early cumulate extracted from such a liquid. This suggests that the websterite has crystallized early enough in the subsolidus history of the peridotite to undergo complete reequilibration of its pyroxene phases. This agrees with the observation that the websterite has been plastically deformed with the surrounding peridotite. We suggest that subsolidus reequilibration after a partial melting event could also account for the lack of mineralogical differences, in the most strongly deformed harzburgites, be-

tween the small interstitial cpx of probable magmatic origin, and the presumably residual cpx porphyroclasts.

#### Origin of Site 670 peridotites: evidences for mantle residues, and evaluation of the degree of partial melting

##### Site 670 peridotites are mantle residues

Bonatti and Hamlyn (1981) divided the ocean-floor peridotites into two groups: (1) ultramafic tectonites probably derived from the upper mantle and (2) ultramafic cumulates probably formed through fractional crystallization of basaltic magma in shallow-level magma chambers. As presented in the previous sections, the modal, textural, and mineralogical characteristics of Site 670 peridotites clearly indicate their affinity with the first group of peridotites, which represents the large majority of ocean-floor peridotites.

Partial melting of the upper mantle under the spinel lherzolite facies conditions and extraction of a basaltic melt is widely accepted as a mechanism that produces ultramafic tectonites as solid residues (Ringwood, 1975; Yoder, 1976; Hamlyn and Bonatti, 1980; Dick et al., 1984). We consider that the chemical composition of the four primary phases of Site 670 peridotites is compatible with a residual origin, particularly their high contents in compatible (or refractory) elements such as Ni, Cr, and Mg, as well as their very low contents in incompatible (or magmaphile) elements such as Ti or Na. Moreover, the porphyroclastic structures systematically developed in these rocks are the result of a high temperature plastic deformation, typical of upper mantle plastic flow conditions (see Cannat et al., this volume). On the other hand, features typical of magmatic cumulates are lacking: no evidence of magmatic layering or of cryptic variations of the mineral phases with their stratigraphic position were observed, nor evidences of any relict of cumulate texture.

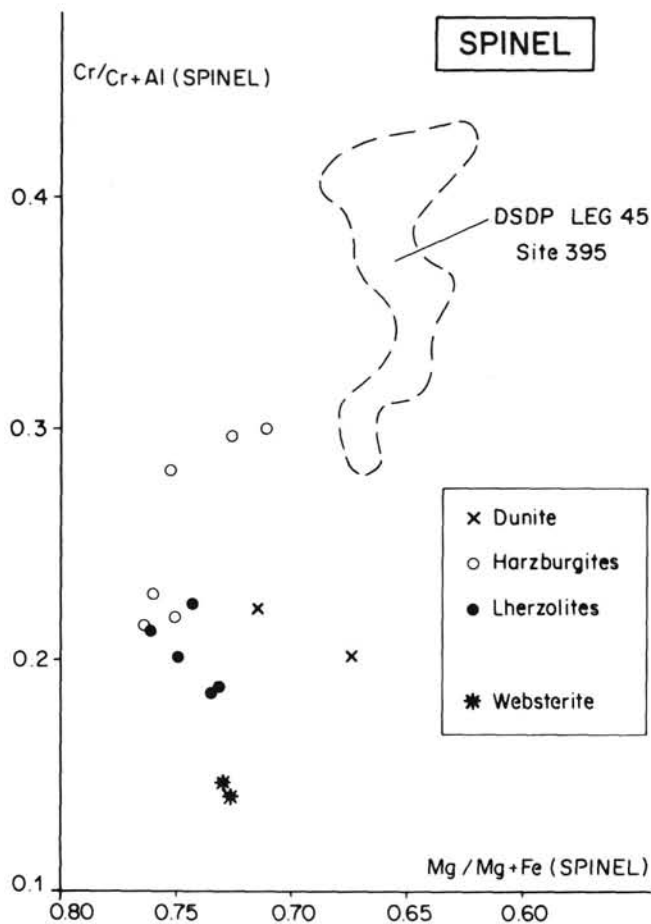


Figure 5. Diagram of the Cr/Cr + Al ratio (or Cr#) vs. the Mg/Mg + Fe ratio (or Mg#) in the spinels of the studied samples, and comparison with Site 395 data. A slight but significant difference appears in the Cr# between the harzburgites (average 24.2) and the lherzolites (average 20.6). The Cr# of the olivine websterite is clearly lower (14.4).

#### Site 670 serpentinized peridotites exhibit indices of partial melting

The presence of numerous and large clusters of pyroxene crystals (opx, cpx), associated with olivine neoblasts, the presence of tiny interstitial cpx crystals, developed by places along planes oriented roughly parallel to the shear plane of the peridotite, and the presence in our sample collection of an olivine websterite, usually interpreted as the "in situ" crystallization of a partial melt trapped in the peridotite matrix (Dick et al., 1984), indicate that Site 670 peridotites were affected by a partial melting event, and that small volumes of the partial melt (or early cumulate crystals extracted from it) were trapped in the peridotites and crystallized along with the solid residue.

#### Estimation of the melting percentage

Theoretical and experimental studies have shown that systematic mineralogical and chemical changes occur in the residue during increasing degrees of partial melting. These modifications include, for a four-phase lherzolitic assemblage: (1) the gradual decrease of modal clinopyroxene (which disappears from the refractory residue after about 15%–25% partial melting) and of modal orthopyroxene, and the correlative increase of modal olivine; (2) a progressive decrease in the magmaphile elements (Ti, Al, Fe and alkalis in the silicate

phases, and Al in spinel), and an increase in the more refractory elements (Mg and Ni in the silicates, Cr in spinel). Thus the Mg# (or Mg/Mg + Fe) of the silicates, the Al content of the pyroxenes, and the Cr# (or Cr/Cr + Al) of spinel are good indicators of the degree of melting and depletion that has occurred in a mantle peridotite (Dick, 1977; Jaques and Green, 1980; Dick and Fisher, 1984).

The Site 670 peridotites show very limited variations in these parameters, confirming that they represent a restricted range in the extent of melting. The fact that mineral compositions are quite identical in the lherzolites, harzburgites, and the dunite of our sample set indicates that the modal variations observed are due to the small size of the samples and to the lithological heterogeneity of the peridotite body, and not to variable degrees of melting.

The melting percentage in Site 670 peridotites is, of course, difficult to estimate precisely, since we ignore the starting composition of the upper mantle before melting. Several lines of evidence, however, point to a moderate melting percentage, probably of the order of 10%–15%:

1. The high contents in  $Al_2O_3$  of the pyroxenes and the spinels, the low Cr# of the spinels, and rather high modal content in cpx (about 5% in average) indicate a moderate percentage of melting. In the diagrams used to define the average trend of the ocean-floor peridotites (Hamlyn and Bonatti, 1980; Dick and Fisher, 1984; Dick and Bullen, 1984; Michael and Bonatti, 1985), the Site 670 peridotites plot toward the least depleted mantle rocks collected in the oceans (see Figs. 4 and 6). Their average composition is close to that collected in the Kane Fracture Zone area (Michael and Bonatti, 1985), where they are associated with N-MORB basalts, and is very different from the average compositions of the peridotites collected at 43°–45°N on the Azores bulge: these peridotites have been shown to be highly residual (their modal composition is very close to the joint ol-opx), and associated with isotopically enriched basalts (Dick et al., 1984; Schilling et al., 1983).

2. The modal composition of the olivine websterite 9R-1, 19–20 cm, may be used to obtain an independent estimation of the degree of melting. If we assume that this sample may approximate the composition of a trapped melt, then we can try to determine graphically the melting percentage using the lever rule. In the ternary modal diagram of Figure 2, we plotted the representative points of Site 670 average peridotite, of the olivine websterite, and of two possible mantle source compositions: the Tinaquillo peridotite (after Jaques and Green, 1980) and the pyrolite of Greenwood (1966). As argued by Jaques and Green (1980), these compositions represent two extreme compositions for suboceanic mantle sources: the Tinaquillo peridotite represents partially depleted, MORB-source mantle, whereas the pyrolite represents an enriched source for intraoceanic islands. Any composition intermediary between both compositions could be a suitable candidate for Site 670 peridotite source. Figure 2 shows that the pyrolite source, Site 670 average peridotite (the residue), and websterite 9R-1, #3 (the melt) plot roughly on the same straight line. The lever rule indicates a melting percentage of about 15%. This number must be taken as a rough estimation, taking into account the uncertainties on the average residue (is our sample set representative of the suboceanic mantle of the area?) and on the melt composition (is our olivine websterite completely representative of a trapped partial melt?). Nevertheless, it is in agreement with the other indications given by mineralogical and modal data.

3. Whole rock compositions of Site 670 peridotites (major and trace elements) also point to intermediary compositions between orogenic lherzolites and ophiolitic harzburgites, and

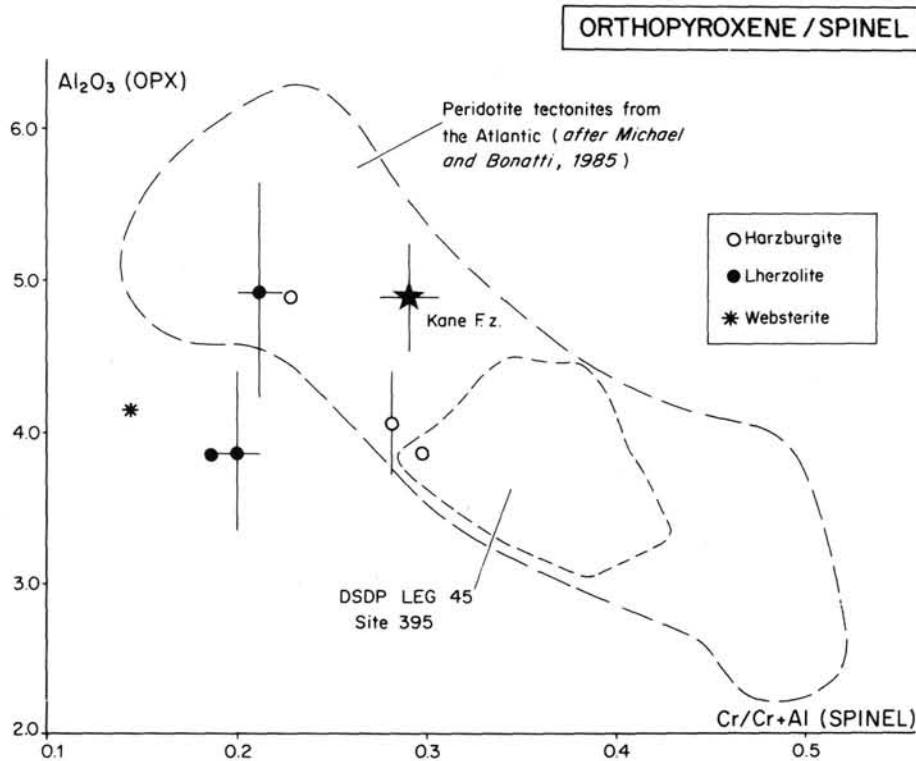


Figure 6. Diagram of the Al<sub>2</sub>O<sub>3</sub> content (wt%) of the orthopyroxenes vs. the Cr/Cr + Al ratio of the spinels in the studied samples, and comparison with other data from the North Atlantic peridotites.

to moderately depleted mantle tectonites (10%–16% of partial melting, after Loubet et al., this volume).

**GEOTHERMOMETRY**

**Sub-solidus equilibrium temperatures**

The equilibrium temperatures and oxygen fugacities have been calculated using the selected microprobe analyses presented in Table 3. These analyses concern the four primary phases (ol, opx, cpx, and sp); individual crystals were ana-

lyzed preferentially in areas where they are in contact with each other. We applied four different geothermometers. The results, obtained in the six samples where at least two geothermometers gave significant results, are summarized in Table 6.

**Choice of the geothermometers**

Most samples show assemblages of four primary phases (olivine, opx, cpx, and Cr-spinel); we could thus apply the following geothermometers:

Table 6. Calculated subsolidus equilibrium temperatures, using the various geothermometers described in the text, and the compositions of olivine, exsolved pyroxenes, and spinel.

Geothermometer	Sample Number					
	4R-1,19-21 cm	5R2,92-94 cm	5R2,142-145 cm	6R1,40-41 cm	6R1,49-51 cm	9R1,19-20 cm
Opx				1074°C (C)		1125°C (C)
Opx-Cpx (Mercier 1976, 1980)		1030°C (C)	1052°C (C)	1090°C (C) 1058°C (C)		1070°C (C)
Cpx			1018°C			
Opx-Cpx (Wood and Banno, 1973)				960°C		
Ol-Opx (Ni = Mg) (Podvin, in press)	1055°C (C) 1058°C (E)	no Opx	1089°C (C) 1059°C	1079°C (C) 960°C	1071°C (C)	1040°C (C) 1121°C (C) 1044°C (C)
Ol-Sp (Fe <sup>2+</sup> = Mg) (Berger and Vannier, 1984)	980°C 955°C 953°C	1014°C (C) 973°C (C)	1022°C (C) 1004°C	999°C (C) 901°C	1006°C (C) 978°C	910°C
Ol-Sp (Si in Sp) (Berger et al., 1982)	1087°C (C) 1060°C 1036°C		1067°C (C)	1177°C (C) 1163°C (C)	1036°C (C) 1067°C	1115°C

(C) = crystal core  
(E) = crystal edge

*Olivine-spinel equilibrium*

Since the work of Jackson (1969), the exchange of  $\text{Fe}^{2+}$  and  $\text{Mg}^{2+}$  cations at equilibrium between olivine and spinel has been calibrated either empirically, using data from natural rocks (Fabries, 1969), or experimentally (Fujii, 1976; Roedder et al., 1979; Sack, 1982; Lehmann, 1983). We use here the geothermometer proposed by Lehmann (1983), tested for ultrabasic rocks by Berger and Vannier (1984).

*Silicon content in spinel*

Stevens (1944), followed by Schlandt and Roy (1965), showed that spinels from peridotites contain silicon. Experimental studies show that the solubility of silicon in spinels is temperature dependent and can thus be used as a geothermometer (Berger et al., 1982; Berger and Vannier, 1984). A comparative study of thermometric data obtained respectively from the Fe-Mg exchange between olivine and spinel, and from the Si content of spinels in a given peridotite suggests that the kinetics of the  $\text{Fe}^{2+}$  and  $\text{Mg}^{2+}$  exchange is rapid, whereas the diffusion of Si in a spinel crystal is a notably slower process (Berger, 1985; Berger and Gelugne, 1987).

*Olivine-opx equilibrium*

Let us call  $K(\text{FM})$  the ratio:  $(\text{Fe}/\text{Mg})_{\text{OL}}:(\text{Fe}/\text{Mg})_{\text{OPX}}$ , and  $K(\text{NM})$  the ratio:  $(\text{Ni}/\text{Mg})_{\text{OL}}:(\text{Ni}/\text{Mg})_{\text{OPX}}$ . It has been shown that, when the temperature increases,  $K(\text{FM})$  remains constant while  $K(\text{NM})$  decreases. The study of several tens of natural peridotites lead to calibrating a geothermometer based on the exchange of Ni and Mg cations between olivine and opx. The proposed geothermometric formula is:

$$\text{TK} = 3820/(\text{Log } K(\text{NM}) + 1.822)$$

and was confirmed by a recent experimental study (Podvin, 1988), with a slight correction of the formula, which becomes:

$$\text{TK} = 3801/(\text{Log } K(\text{NM}) + 1.815)$$

If the pair olivine-opx is itself in equilibrium with a spinel, it is possible to calculate the oxygen fugacity in the system at the equilibrium temperature (Vannier, 1977).

*Opx-cpx equilibrium*

The well-known pyroxenic geothermometers used in this paper are those of Wood and Banno (1973) and of Mercier (1976, 1980). The former, which needs the presence of both types of pyroxenes, was difficult to use in this study either because of the absence of one of the pyroxenes in the thin section, or because of the widespread occurrence of tiny exsolution lamellae in both types of pyroxene crystals. Thus, we mostly used the "one pyroxene" geothermometers of Mercier and got the last subsolidus equilibrium temperatures recorded in the peridotites before serpentinization.

**Results**

Table 6 gives the subsolidus equilibrium temperatures obtained using the different geothermometers. These temperatures are relatively high, generally around 1000°C. The highest ones are given by the Si content in spinels, whereas the lowest temperatures are given by the olivine/spinel geothermometer, in agreement with the difference in the kinetics of the exchange reactions involved. Therefore, the equilibrium temperatures indicated by the "Si" method should be closer to the magmatic equilibrium temperatures which prevailed in these rocks at the end of the partial melting events (before exsolution in pyroxenes), and the temperatures indicated by the olivine/spinel method should reflect the subsoli-

du blocking temperatures recorded in the peridotites during their ascent toward the surface and before the development of serpentinization. These blocking temperatures are unusually high, close to 1000°C, indicating that the peridotite body was cooled rapidly, starting from a melting zone equilibrated at a temperature above 1180°C (Table 6).

The oxygen fugacities were calculated for a pressure of 10 kb and at the temperature indicated by the ol/sp geothermometer (generally between 950°C and 1000°C, see Table 6), using the method described by Vannier (1977). Based on the ol-opx-sp equilibrium, the Vannier's method was tested and calibrated on peridotite inclusions in alkali basalts from French Massif-Central and Polynesia: in these inclusions impregnated by the host alkali-basalts and reequilibrated with them, the  $f\text{O}_2$  calculated with the Vannier's method in the ultramafic inclusions plot on the same FMQ buffer as the  $f\text{O}_2$  calculated in the basalts from ilmenite-magnetite pairs (Berger, 1981). In our rocks, these fugacities range from about  $10^{-10.6}$  to  $10^{-11.2}$  for the peridotites (Table 7); they are quite comparable to the oxygen fugacities commonly calculated in ophiolitic mantle peridotites or in peridotite nodules, and plot on the FMQ buffer (Fig. 7).

**Partial melting temperatures, given by the "primitive" composition of the pyroxene porphyroclasts**

The numerous exsolution lamellae frequently observed in both opx and cpx porphyroclasts indicate that the temperatures previously inferred from the porphyroclast and exsolved compositions reflect subsolidus rather than magmatic equilibration. Admitting that the presence of diopside lamellae in opx porphyroclasts, and of enstatite lamellae in cpx porphyroclasts, is the result of the subsolidus evolution of the studied peridotites, their "integration" in the overall composition of the host-pyroxene may give a good idea of their solidus (or magmatic) composition, and of the temperatures at which these pyroxenes were equilibrated at the end of the main melting episode.

We tried to accomplish this "integration" doing microprobe manual traverses across the cores of opx and cpx porphyroclasts, avoiding their recrystallized margins and selecting sections where the exsolved lamellae are roughly perpendicular to the plane of the thin section (minimum width and sharpness of their margins are good criteria). Each traverse includes punctual analyses with 10  $\mu\text{m}$  spacing and a counting time of 8 min. Other analytical conditions are identical to those indicated for Table 3.

The analytical results are given in Table 8. They must be taken with caution: the analyzed sections exhibit variable contents in exsolution lamellae, themselves having variable orientations with respect to the plane of the thin section, in spite of the precautions taken. We found numerous opx sections presenting favorable sections, with abundant and thin lamellae, regularly spaced and well oriented (perpendicular to the thin section plane). The cpx sections appeared to have less exsolution lamellae more irregularly spaced and more variably oriented. These observations are reflected in Table 8. Opx "primitive" compositions are very homogeneous and clustered around the average value, with the exception of three of them falling in the subsolidus field; they have slightly higher contents in  $\text{Al}_2\text{O}_3$  (3.64%–6.07%, average 4.37%), in CaO (1.08%–2.18%, average 1.77%), in wollastonite molecule (Wo 2.09%–4.28%, average 3.46%), and Mg# (90.8 in average) than the exsolved porphyroclasts. Cpx "primitive" compositions are much more variable, showing a Wo content ranging from about 41% to 46%, with an average of 43.17%. They have slightly higher contents in  $\text{Al}_2\text{O}_3$  (5.81%–6.03%, average 5.92%) and in  $\text{Cr}_2\text{O}_3$  (average 1.16%) than the exsolved

**Table 7. Oxygen fugacities calculated for 10 kb pressure at 1000°C and at 1200°C, using the ol-opx-sp equilibrium (Vannier, 1977). C = using analyses of the cores of minerals, in clusters of the three phases. M = using analyses of the margins of the minerals (numbers refer to the clusters analyzed).**

Sample Number	Cores or margins	fO <sub>2</sub> calculated for:	
		10Kb, 1000°C	10Kb, 1200°C
4R1, 19-21 cm	C	10 <sup>-10.82</sup>	10 <sup>-8.43</sup>
5R1, 2-6 cm	C	10 <sup>-11.18</sup>	10 <sup>-8.87</sup>
5R1, 2-6 cm	M	10 <sup>-11.16</sup>	10 <sup>-8.84</sup>
5R2, 142-145 cm	C1	10 <sup>-10.57</sup>	10 <sup>-8.20</sup>
5R2, 142-145 cm	C2	10 <sup>-10.89</sup>	10 <sup>-8.53</sup>
6R1, 40-41 cm	C1	10 <sup>-10.41</sup>	10 <sup>-8.08</sup>
6R1, 40-41 cm	C2	10 <sup>-10.02</sup>	10 <sup>-8.7</sup>
6R1, 49-51 cm	C1	10 <sup>-10.6</sup>	10 <sup>-8.26</sup>
6R1, 49-51 cm	C2	10 <sup>-11.2</sup>	10 <sup>-8.88</sup>
7R1, 17-18 cm	C	10 <sup>-10.76</sup>	10 <sup>-8.42</sup>
7R1, 17-18 cm	M	10 <sup>-10.7</sup>	10 <sup>-8.36</sup>
9R1, 19-20 cm	C1	10 <sup>-10.83</sup>	10 <sup>-8.54</sup>
9R1, 19-20 cm	C2, 3	10 <sup>-10.98</sup>	10 <sup>-8.69</sup>
9R1, 19-20 cm	M2, 3	10 <sup>-10.8</sup>	10 <sup>-8.51</sup>

porphyroclasts, and lower contents in TiO<sub>2</sub> (average 0.13) and CaO (average 20.66%), the Mg# remaining identical (90.7 in average).

We analyzed also the pyroxenes of the websterite 9R-1, 19–20 cm (Table 8), which appear to have “primitive” compositions very close to those of the surrounding peridotites, with the notable exception of their Cr content, which is clearly lower.

For most of the analyses done, the temperatures calculated with the single pyroxene geothermometer of Mercier (1980) are between 1290°C and 1320°C for the “primitive” opx, and about 100°C lower (around 1200°C) for the “primitive” cpx. For example, the pyroxenes of Sample 7R-1, 17–18 cm, give respectively 1303°C for the “primitive” opx and 1166°C for the “primitive” cpx. The “primitive” pyroxenes of the olivine websterite give the same range of temperatures: 1320°C for the opx and 1161°C for the cpx.

In summary, the recalculated “primitive” compositions of the pyroxene porphyroclasts in the studied samples lead to the following conclusions:

1. The opx porphyroclasts, characterized by abundant and regularly spaced diopside lamellae and by very homogeneous compositions statistically, lead to calculated temperatures of crystallization probably very close to the actual temperatures of equilibrium at the end of the main partial melting episode, that is, close to about 1300°C.

2. The cpx porphyroclasts, characterized by scarcer and less regularly spaced enstatite lamellae, exhibit a wider range of “primitive” compositions (even in a same sample, as well as from one sample to another). The temperatures calculated are about 100°C lower than for “primitive” opx, indicating that their recalculated compositions are not at equilibrium with those of the “primitive” opx, probably because of a more complex history during the melting events.

3. The comparison between the “primitive” pyroxenes from the peridotites and from the olivine websterite 9R-1, 19–20 cm, suggests that these rocks have followed together the same thermal evolution, starting from the very end of the main melting event, when these rocks were equilibrated together at high temperatures for the first time.

## SUMMARY AND CONCLUSIONS

About 100 m of serpentinized, residual mantle tectonites outcropping along the western wall of the M.A.R. axial rift valley, 45 km south of the Kane Fracture Zone, were drilled

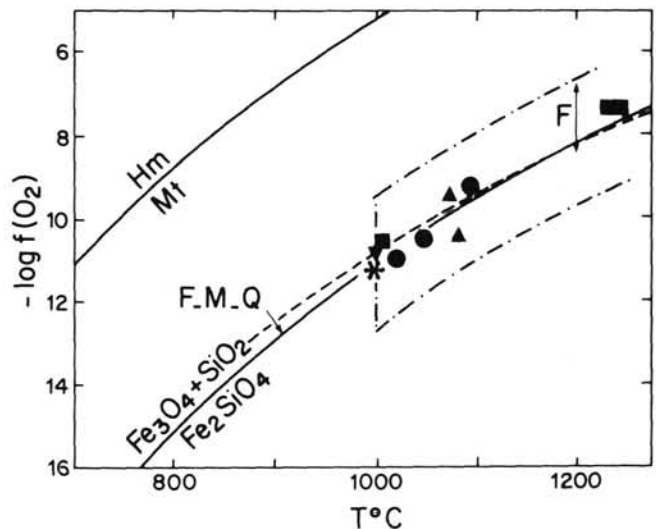


**Figure 7. Oxygen fugacities calculated in the Site 670 peridotites for 10 kb pressure and at the blocking temperatures indicated by the olivine/spinel geothermometer (Table 6), close to 1000°C. The oxygen fugacities obtained for Site 670 peridotites, represented by the black inverted triangle (average of values given in Table 7), are compared with the fugacities calculated for some other oceanic peridotites (black circles = peridotites from ophiolitic massifs; other symbols = peridotite inclusions in alkali basalts).**

during ODP Leg 109 at Site 670. Twenty-nine small pieces of these ultramafic rocks, sampled along the 6.12 m of core recovered, were examined for petrographic description, and nine samples were selected for detailed mineralogical study of their primary phases.

The main conclusions of the present study may be summarized as follows:

1. The sample collection includes about 60% serpentinized harzburgites, 26% serpentinized lherzolites, 14% serpentinized dunites, and one sample of olivine websterite. Serpentine-free modal analyses of the nine selected samples have shown that all these rocks are plagioclase-free four-phase peridotites equilibrated in the spinel lherzolite facies (ol + opx + cpx + sp).

2. Among the nine selected samples, eight represent serpentinized (53%–78%) residual upper mantle tectonites ranging from dunitic to harzburgitic and lherzolitic compositions. The last sample is a rather fresh olivine websterite showing the same porphyroclastic texture as the peridotites. This rock could represent an early crystallization product (cumulate?) of a trapped liquid produced during a partial melting event.

3. The compositional variations of olivine, opx, and cpx are restricted and do not correlate with changes in the modal composition. Only the spinel phase is sensitive to modal changes, having a slightly higher Cr# in the harzburgite and dunite samples. We assume that the degree of partial melting in Site 670 peridotites was roughly the same everywhere, with perhaps small, second order variations recorded in the spinel Cr#.

4. The average modal composition of our sample collection (about ol 80%, opx 14%, cpx 5%, and sp 1%), the porphyroclastic textures, and the mineralogical characteristics of Site 670 peridotites clearly indicate their affinity with the ultramafic mantle tectonites. Features typical of magmatic cumulates are lacking.

5. The high contents in Al<sub>2</sub>O<sub>3</sub> of the pyroxene and of the spinel phases, the low Cr# of the spinels, and the rather high

**Table 8. Recalculated compositions of the “primitive” pyroxenes, obtained by microprobe traverses across the cores of the opx and cpx porphyroclasts, in order to integrate the exsolution lamellae in the host-crystals. Temperatures calculated from these compositions are discussed in the text.**

Sample Nber	4R1,#3	4R1,#3	4R1,#3	5R1,#1	5R2,19	5R2,#19	5R2,#19	6R1,#6	6R1,#6	6R1,#8	6R1,#8	6R1,#8
Mineral	Opx-1	Opx-1	Opx-1	Opx-1	Opx-1	Opx-1	Opx-1	Opx-2	Opx-2	Opx-1	Opx-2	Opx-2
Anal. Nber	PT 778	PT 777	PT 776	PT 772	PT 771	PT 770	PT 768	PT 767	PT 763	PT 754	PT 753	PT 752
SiO <sub>2</sub>	55.53	54.55	55.24	55.07	54.63	54.70	54.82	55.53	55.39	55.59	54.13	54.43
TiO <sub>2</sub>	0.06	0.08	0.07	0.05	0.09	0.10	0.07	0.04	0.05	0.05	0.05	0.07
Al <sub>2</sub> O <sub>3</sub>	3.64	4.04	3.80	4.17	4.69	4.54	4.81	4.21	4.34	3.86	4.83	4.74
Cr <sub>2</sub> O <sub>3</sub>	0.81	0.89	0.78	0.60	0.89	0.92	0.99	0.64	0.72	0.42	0.86	0.84
FeO	5.60	5.77	5.68	5.93	5.80	5.66	5.74	5.90	5.91	6.07	5.73	5.92
MnO	0.14	0.13	0.14	0.14	0.13	0.14	0.15	0.13	0.14	0.12	0.13	0.15
MgO	32.64	32.87	32.57	32.68	31.84	31.97	31.82	32.78	32.53	32.95	32.02	31.68
CaO	1.96	1.85	1.71	1.30	2.09	2.02	1.87	1.16	1.08	1.08	2.07	2.18
Na <sub>2</sub> O	0.08	0.04	0.05	0.00	0.03	0.04	0.03	0.01	0.01	0.01	0.01	0.00
K <sub>2</sub> O	0.01	0.00	0.00	0.01	0.01	0.00	0.00	0.00	0.00	0.00	0.00	0.00
NiO	0.09	0.09	0.11	0.09	0.11	0.10	0.1	0.10	0.11	0.10	0.10	0.10
Total	100.56	100.31	100.15	100.04	100.31	100.19	100.41	100.50	100.28	100.25	99.93	100.11
Si	1.910	1.879	1.908	1.903	1.888	1.892	1.893	1.910	1.911	1.916	1.875	1.886
AlIV	0.090	0.121	0.092	0.097	0.112	0.108	0.107	0.090	0.089	0.084	0.125	0.114
AlVI	0.058	0.043	0.063	0.073	0.079	0.077	0.089	0.081	0.088	0.073	0.072	0.080
Ti	0.002	0.002	0.002	0.001	0.002	0.003	0.002	0.001	0.001	0.001	0.001	0.002
Cr	0.022	0.024	0.021	0.016	0.024	0.025	0.027	0.017	0.020	0.011	0.024	0.023
Fe <sup>3+</sup>	0.013	0.052	0.008	0.006	0.006	0.004	0.000	0.000	0.000	0.000	0.027	0.008
Fe <sup>2+</sup>	0.148	0.114	0.156	0.166	0.161	0.159	0.166	0.170	0.171	0.175	0.139	0.164
Mn	0.004	0.004	0.004	0.004	0.004	0.004	0.004	0.004	0.004	0.004	0.004	0.004
Mg	1.673	1.687	1.676	1.683	1.640	1.648	1.638	1.681	1.673	1.693	1.653	1.636
Ca	0.072	0.068	0.063	0.048	0.077	0.075	0.069	0.043	0.040	0.040	0.077	0.081
Na	0.005	0.003	0.003	0.000	0.002	0.003	0.002	0.001	0.001	0.001	0.001	0.000
K	0.000	0.000	0.000	0.000	0.000	0.000	0.000	0.000	0.000	0.000	0.000	0.000
Ni	0.002	0.002	0.003	0.003	0.003	0.003	0.003	0.003	0.003	0.003	0.003	0.003
Total	4.000	4.000	4.000	4.000	4.000	4.000	4.000	4.000	4.000	4.000	4.000	4.000
Mg/Mg+Fe	91.20	91.03	91.09	90.76	90.73	90.96	90.81	90.83	90.75	90.63	90.87	90.51
Wo	3.79	3.55	3.32	2.53	4.11	3.97	3.70	2.26	2.12	2.09	4.05	4.29
En	87.76	87.80	88.06	88.46	87.00	87.35	87.45	88.77	88.82	88.74	87.19	86.63
Fs	8.45	8.65	8.62	9.01	8.89	8.88	8.85	8.97	9.06	9.17	8.76	9.08

Sample Nber	7R1,#3	7R1,#3	7R1,#3	Opx	5R1,#1	5R1,#1	5R1,#1	6R1,#6	6R1,#8	6R1,#8	6R1,#8	7R1,#2
Mineral	Opx-1	Opx-1	Opx-1	Average	Cpx-1	Cpx-1	Cpx-1	Cpx-2	Cpx-3	Cpx-3	Cpx-3	Cpx-1
Anal. Nber	PT 784	PT 783	PT 782	PT 775	PT 774	PT 773		PT 765	PT 751	PT 750	PT 748	PT 779
SiO <sub>2</sub>	54.27	54.13	54.48	54.83	50.96	51.25	51.19	51.00	50.52	51.73	51.00	51.01
TiO <sub>2</sub>	0.05	0.05	0.06	0.06	0.14	0.14	0.13	0.15	0.11	0.13	0.13	0.12
Al <sub>2</sub> O <sub>3</sub>	4.60	4.69	4.57	4.37	5.92	5.88	5.92	5.81	5.86	5.99	6.00	5.97
Cr <sub>2</sub> O <sub>3</sub>	0.73	0.74	0.81	0.78	1.22	1.13	1.06	1.28	1.12	1.06	1.24	1.14
FeO*	5.92	5.85	5.99	5.83	3.20	3.16	3.24	2.92	3.52	3.30	3.15	3.35
MnO	0.14	0.15	0.14	0.14	0.13	0.10	0.11	0.09	0.12	0.12	0.13	0.09
MgO	31.73	31.77	31.96	32.25	17.29	18.17	17.45	16.89	17.56	18.31	17.71	18.37
CaO	2.18	2.09	1.96	1.772	1.38	20.02	21.12	21.92	21.12	19.54	20.59	19.83
Na <sub>2</sub> O	0.02	0.02	0.00	0.02	0.16	0.11	0.15	0.19	0.16	0.17	0.17	0.18
K <sub>2</sub> O	0.01	0.01	0.00	0.00	0.00	0.00	0.00	0.00	0.00	0.00	0.00	0.00
NiO	0.10	0.11	0.09	0.10	0.06	0.08	0.09	0.06	0.07	0.08	0.05	0.09
Total	99.75	99.61	100.06	100.16	100.46	100.04	100.46	100.31	100.16	100.43	100.17	100.15
Si	1.885	1.882	1.887	1.895	1.839	1.852	1.846	1.845	1.827	1.861	1.842	1.839
AlIV	0.115	0.118	0.113	0.105	0.161	0.148	0.154	0.155	0.173	0.139	0.158	0.161
AlVI	0.074	0.075	0.074	0.073	0.091	0.102	0.098	0.093	0.077	0.115	0.098	0.093
Ti	0.001	0.001	0.002	0.002	0.004	0.004	0.004	0.004	0.003	0.004	0.004	0.003
Cr	0.020	0.020	0.022	0.021	0.035	0.032	0.030	0.037	0.032	0.030	0.035	0.032
Fe <sup>3+</sup>	0.020	0.022	0.014	0.009	0.038	0.014	0.029	0.031	0.069	0.000	0.029	0.042
Fe <sup>2+</sup>	0.152	0.148	0.159	0.159	0.058	0.081	0.069	0.058	0.037	0.099	0.066	0.059
Mn	0.004	0.004	0.004	0.004	0.004	0.003	0.003	0.003	0.004	0.004	0.004	0.003
Mg	1.643	1.646	1.650	1.661	0.930	0.978	0.938	0.911	0.946	0.982	0.954	0.987
Ca	0.081	0.078	0.073	0.066	0.827	0.775	0.816	0.850	0.818	0.753	0.797	0.766
Na	0.001	0.001	0.000	0.002	0.011	0.008	0.010	0.013	0.011	0.012	0.012	0.013
K	0.000	0.000	0.000	0.000	0.000	0.000	0.000	0.000	0.000	0.000	0.000	0.000
Ni	0.003	0.003	0.003	0.003	0.002	0.002	0.003	0.002	0.002	0.002	0.001	0.003
Total	4.000	4.000	4.000	4.000	4.000	4.000	4.000	4.000	4.000	4.000	4.000	4.000
Mg/Mg+Fe	90.52	90.63	90.48	90.79	90.59	91.11	90.56	91.16	89.89	90.82	90.92	90.72
Wo	4.28	4.11	3.84	3.46	44.61	41.92	44.07	45.96	43.73	41.07	43.18	41.32
En	86.65	86.91	87.01	87.64	50.18	52.92	50.65	49.26	50.58	53.52	51.66	53.24
Fs	9.07	8.98	9.15	8.89	5.21	5.16	5.28	4.78	5.69	5.41	5.16	5.45

Sample Nber	7R1,#2	7R1,#2	Cpx	9R1,#3	9R1,#3	Web.Cpx	9R1,#3	9R1,#3	9R1,#3	Web.Opx
Mineral	Cpx-1	Cpx-1	Average	Cpx-2	Cpx-2	Average	Opx-1	Opx-1	Opx-3	Average
Anal. Nber	PT 780	PT 781	PT 762	PT 758			PT 755	PT 756	PT 757	
SiO <sub>2</sub>	50.99	50.76	51.04	51.11	51.58	51.35	54.955	5.22	55.22	55.13
TiO <sub>2</sub>	0.13	0.12	0.13	0.12	0.10	0.11	0.05	0.05	0.04	0.05
Al <sub>2</sub> O <sub>3</sub>	5.81	6.03	5.92	5.17	5.03	5.10	4.04	4.14	4.09	4.09
Cr <sub>2</sub> O <sub>3</sub>	1.16	1.21	1.16	0.63	0.61	0.62	0.46	0.43	0.44	0.44

Table 8 (continued).

Sample Nber	7R1,#2	7R1,#2	Cpx	9R1,#3	9R1,#3	Web.Cpx	9R1,#3	9R1,#3	9R1,#3	Web.Opx
FeO*	3.08	3.33	3.23	2.98	2.87	2.93	5.46	5.61	5.57	5.55
MnO	0.11	0.13	0.11	0.13	0.11	0.12	0.15	0.16	0.15	0.15
MgO	17.44	18.20	17.74	17.62	17.75	17.69	32.07	32.32	32.26	32.22
CaO	21.04	20.01	20.66	21.92	21.79	21.86	2.64	1.99	2.29	2.31
Na <sub>2</sub> O	0.19	0.15	0.16	0.16	0.16	0.16	0.02	0.03	0.01	0.02
K <sub>2</sub> O	0.00	0.00	0.00	0.01	0.00	0.01	0.00	0.00	0.00	0.00
NiO	0.07	0.07	0.07	0.08	0.08	0.08	0.11	0.10	0.12	0.11
Total	100.02	100.01	100.00	99.93	100.08	100.01	99.95	100.05	100.19	100.06
Si	1.846	1.834	1.843	1.850	1.863	1.856	1.902	1.908	1.907	1.906
AlIV	0.154	0.166	0.157	0.150	0.137	0.144	0.098	0.092	0.093	0.094
AlVI	0.094	0.091	0.095	0.070	0.077	0.074	0.067	0.077	0.073	0.072
Ti	0.004	0.003	0.004	0.003	0.003	0.003	0.001	0.001	0.001	0.001
Cr	0.033	0.035	0.033	0.018	0.017	0.018	0.013	0.012	0.012	0.012
Fe <sup>3+</sup>	0.033	0.045	0.033	0.067	0.048	0.058	0.017	0.002	0.007	0.009
Fe <sup>2+</sup>	0.060	0.056	0.064	0.023	0.039	0.031	0.141	0.160	0.154	0.152
Mn	0.003	0.004	0.003	0.004	0.003	0.004	0.004	0.005	0.004	0.004
Mg	0.941	0.980	0.955	0.950	0.956	0.953	1.654	1.665	1.660	1.660
Ca	0.816	0.775	0.799	0.850	0.843	0.847	0.098	0.074	0.085	0.085
Na	0.013	0.011	0.011	0.011	0.011	0.011	0.001	0.002	0.001	0.001
K	0.000	0.000	0.000	0.000	0.000	0.000	0.000	0.000	0.000	0.000
Ni	0.002	0.002	0.002	0.002	0.002	0.002	0.003	0.003	0.003	0.003
Total	4.000	4.000	4.000	4.000	4.000	4.000	4.000	4.000	4.000	4.000
Mg/Mg+Fe	90.98	90.69	90.74	91.33	91.68	91.51	91.28	91.12	91.17	91.19
Wo	44.11	41.75	43.17	44.96	44.73	44.84	5.13	3.88	4.45	4.48
En	50.85	52.82	51.57	50.27	50.68	50.47	86.60	87.59	87.11	87.10
Fs	5.04	5.42	5.26	4.77	4.60	4.68	8.27	8.53	8.44	8.42

modal content in cpx indicate a moderate percentage of melting, of the order of 10%–15%. Site 670 peridotites plot close to the least depleted mantle rocks collected in the oceans, in most diagrams used to define the average trend of the ocean-floor peridotites.

6. Independently, a graphical method using the modal composition of the olivine websterite sample, of the residue (average of Site 670 peridotites), and of possible mantle sources also indicates a melting percentage of about 15%.

7. The thermal evolution of Site 670 peridotites in the high temperature field may be summarized as follows: the magmatic temperatures of melting are best recorded in the recalculated "primitive" opx porphyroclasts, which indicate a temperature of about 1300°C. The "primitive" cpx were more sensitive to reactions with trapped melts and subsequent deformation/recrystallization episodes, and record lower temperatures of about 1200°C. The subsolidus evolution is well recorded, from about 1200°C to 950°C, by the exsolved opx and cpx porphyroclasts and the other phases (ol, sp) in equilibrium with them. High subsolidus temperatures are recorded by the "Si" geothermometer (using the Si content in spinel), and the lowest blocking temperatures are indicated by the ol/sp geothermometer. These blocking temperatures are high (close to 1000°C), indicating that the peridotite body was cooled very rapidly between 1000°C and the beginning of serpentinization around 500°C.

8. In the normative ol-opx-cpx diagram, the composition of the olivine websterite plots close to the 8 kb melting point determined experimentally (Takahashi and Kushiro, 1983). This may indicate that at the end of the main melting episode, the depth reached by the peridotite body was 25–30 km approximately.

9. Oxygen fugacities calculated for a pressure of 10 kb and at the blocking temperatures indicated by the ol/sp geothermometer (about 1000°C), indicate fugacities of the order of  $10^{-10.6}$  to  $10^{-11.2}$ , usual in upper mantle peridotites of oceanic origin.

10. Site 670 peridotites have compositions close to those of the peridotites collected in the Kane Fracture Zone, and obviously belong to the moderately depleted mantle peridotites

which characterize abyssal peridotites collected away from mantle plumes and oceanic islands. In particular, they differ considerably from the highly residual harzburgites collected along the M.A.R. over the Azores bulge between 43° and 45° N.

#### REFERENCES

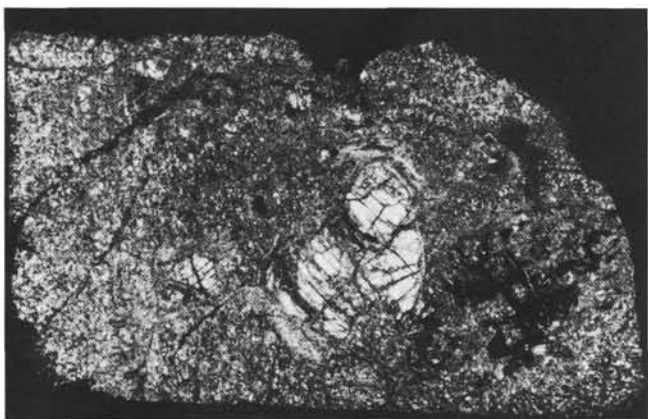
- Berger, E. T., 1981. Enclaves ultramafiques, mégacristaux et leurs basaltes hôtes en contexte océanique (Pacifique sud) et continental (Massif-Central français). [Ph.D. dissert.] Univ. Paris 11.
- , 1985. Hétérogénéités pétrographiques du manteau Sud-Pacifique, sous l'archipel des Australes: mise en évidence et interprétation par l'étude des enclaves ultramafiques. *Bull. Soc. Géol. Fr.*, 2:207–216.
- Berger, E. T., Frot, G., Lehmann, J., Marion, C., and Vannier, M., 1982. Un géothermomètre potentiel très sensible, reposant sur la teneur en silicium des spinelles de paragenèses à olivine. *C. R. Acad. Sci., Paris*, 294:733–736.
- Berger, E. T., and Vannier, M., 1984. Les dunites en enclaves dans les basaltes des océaniques: approche pétrologique. *Bull. Minéral.*, 107:649–663.
- Berger, E. T., and Gelugne P., 1987. Première découverte, à Tahiti, de harzburgites mantelliques en enclaves dans une coulée basaltique. *C. R. Acad. Sci., Paris*, 304:903–906.
- Bonatti, E., and Hamlyn, P. R., 1981. Oceanic ultramafic rocks. In Emiliani, C., (Ed.), *The Sea, the oceanic lithosphere*, vol. 7, New York (Wiley), 241–283.
- Boudier, F., and Nicolas, A., 1972. Fusion partielle gabbroïque dans la lherzolite de Lanzo (Alpes piémontaises). *Schweiz. Mineral. Petrog. Mitt.*, 52:39–56.
- Bryan, W. B., Thompson, G., and Ludden, J. N., 1981. Compositional variation in normal MORB from 22°–25°N: Mid-Atlantic Ridge and Kane Fracture Zone. *J. Geophys. Res.*, 86: 11815–11836.
- Cormier, M. H., Detrick, R. S., and Purdy, G. M., 1984. Anomalous thin crust in oceanic fracture zones; new seismic constraints from the Kane fracture zone. *J. Geophys. Res.*, 89: 10244–10266.
- Detrick, R. S., and Purdy, G. M., 1980. The crustal structure of the Kane Fracture Zone. *J. Geophys. Res.*, 85:3759–3778.
- Detrick, R. S., Ryan, W.B.F., Mayer, L., Fox, P. J., Kong, L., Manchester, K., Kastens, K., Karson, J., and Pockalny, R., 1985. *Mid-Atlantic Ridge/Kane Fracture Zone Final Site Survey Report*. Prepared for Joint Oceanographic Institutions Inc.

- Dick, H.J.B., 1977. Partial melting in the Josephine Peridotite. I, the effect on mineral composition and its consequence for geobarometry and geothermometry. *Am. J. Sci.*, 277:801–832.
- Dick, H.J.B., and Fisher, R. L., 1984. Mineralogic studies of the residues of mantle melting: abyssal and alpine-type peridotites. In Kornprobst, J. (Ed.), *Kimberlites II: The Mantle and Crust-Mantle Relationships*, Amsterdam (Elsevier), 295–308.
- Dick, H.J.B., and Bullen, T., 1984. Chromian spinel as a petrogenetic indicator in abyssal and alpine-type peridotites and spatially associated lavas. *Contrib. Mineral. Petrol.*, 86:54–76.
- Dick, H.J.B., Fisher, R. L., and Bryan, W. B., 1984. Mineralogic variability of the uppermost mantle along mid-ocean ridges. *Earth Planet. Sci. Lett.*, 69:88–106.
- Fabries, J., 1969. Spinel-olivine geothermometry in peridotites from ultramafic complexes. *Contrib. Mineral. Petrol.*, 69:329–336.
- Fujii, T., 1976. Fe-Mg partitioning between olivine and spinel. *Carnegie Inst. Washington, Yearb.*, 76:563–569.
- Hamlyn, P. R., and Bonatti, E., 1980. Petrology of mantle derived ultramafics from the Owen Fracture Zone, northwest Indian ocean: implications for the nature of the oceanic upper mantle. *Earth Planet. Sci. Lett.*, 48:65–79.
- Jackson, E. D., 1969. Chemical variation in coexisting chromite and olivine in the chromitite zones of the Stillwater complex. *Econ. Geol. Mon.*, 4:41–71.
- Jaques, A. L., and Green, D. H., 1980. Anhydrous melting of peridotite at 0–15 kb pressure and the genesis of tholeiitic basalts. *Contrib. Mineral. Petrol.*, 73:287–310.
- Karson, J. A., and Dick, H.J.B., 1983. Tectonics of ridge-transform intersections at the Kane Fracture Zone. *Mar. Geophys. Res.*, 6:51–98.
- Karson, J. A., Thompson, G., Humphris, S. E., Edmond, J. M., Bryan, W. B., Brown, J. R., Winters, A. T., Pockalny, R. A., Casey, J. F., Campbell, A. C., Klinkhammer, G., Palmer, M. R., Kinzler, R. J., and Sulanowska M. M., 1987. Along-axis variations in seafloor spreading in the MARK area. *Nature*, 328:681–685.
- Lehmann, J., 1983. Diffusion between olivine and spinel: application to geothermometry. *Earth Planet. Sci. Lett.*, 64:123–138.
- Le Sueur, E., Boudier, F., Cannat, M., Ceuleneer, G., and Nicolas A., 1984. The Trinity mafic-ultramafic complex: first results of the structural study of an atypical ophiolite. *Ophioliti*, 9:487–498.
- Marion, C., and Vannier, M., 1983. Dosage par double mesure au micro-analyseur à sonde électronique automatisée. *J. Microsc. Spectrosc. Electron.*, 8:31–46.
- Melson, W. G., Thompson, G., and Van Andel, T. H., 1968. Volcanism and metamorphism in the Mid-Atlantic Ridge, 22°N Latitude. *J. Geophys. Res.*, 73:5925–5941.
- Mercier, J. C., 1976. Single pyroxene geothermometry and geobarometry. *Am. Miner.*, 61:603–615.
- \_\_\_\_\_, 1980. Single pyroxene thermobarometry. *Tectonophysics*, 70:1–37.
- Mercier, J. C., and Nicolas, A., 1975. Textures and fabrics of upper mantle peridotites as illustrated by xenoliths from basalts. *J. Petrol.*, 16:454–496.
- Michael, P. J., and Bonatti, E., 1985. Peridotite composition from the North Atlantic: regional and tectonic variations and implications for partial melting. *Earth Planet. Sci. Lett.*, 73:91–104.
- Nicolas, A., and Jackson, M., 1982. High temperature dikes in peridotites: origin by hydraulic fracturing. *J. Petrol.*, 23:568–582.
- Pockalny, R. A., Detrick, R. S., and Fox, P. J., in press. The morphology and tectonics of the Kane transform fault from Sea Beam bathymetry data. *J. Geophys. Res.*
- Podvin, P., in press. Ni-Mg partitioning between synthetic olivines and orthopyroxenes: application to geothermometry. *Am. Miner.*
- Purdy, G. M., Rabinowitz, P. D., and Schouten, H., 1978. The Mid-Atlantic Ridge at 23°N: bathymetry and magnetics. In Melson, W. G., Rabinowitz, P. D., et al., *Init. Repts. DSDP*, 45: Washington (U.S. Govt. Printing Office), 119–128.
- Purdy, G. M., and Detrick, R. S., 1986. Crustal structure of the Mid-Atlantic Ridge at 23°N from seismic refraction studies. *J. Geophys. Res.*, 91:3739–3762.
- Ringwood, A. E., 1966. Composition and origin of the earth. In Hurley, P. M. (Ed.) *Advances in Earth Sciences*: Cambridge (MIT Press), 287–356.
- \_\_\_\_\_, 1975. *Composition and Petrology of the Earth's Mantle*. New York (McGraw-Hill).
- Roeder, P. L., Campbell, I. H., and Jamieson, H. E., 1979. A re-evaluation of the Olivine-Spinel Geothermometer. *Contrib. Mineral. Petrol.*, 68:325–334.
- Sack, R. O., 1982. Spinel as petrogenetic indicators: activity-composition relations at low pressures. *Contrib. Mineral. Petrol.*, 79:169–186.
- Schilling, J. G., Zajac, M., Evans, R., Johnston, T., White, W., Devine, J. D., and Kingsley, R., 1983. Petrologic and geochemical variations along the Mid-Atlantic Ridge from 29°N to 73°N. *Am. J. Sci.*, 510–586.
- Schlaudt, C. M., and Roy, D. M., 1965. Crystalline solution in the system MgO-Mg<sub>2</sub>SiO<sub>4</sub>-MgAl<sub>2</sub>O<sub>4</sub>. *J. Am. Ceram. Soc.*, 48:248–251.
- Stevens, R. E., 1944. Composition of some chromites of the western hemisphere. *Am. Miner.*, 29:1–34.
- Takahashi, E., and Kushiro, I., 1983. Melting of a dry peridotite at high pressures and basalt magma genesis. *Am. Mineral.*, 68:859–879.
- Vannier, M., 1977. Modélisation de la solution solide spinelle naturelle. *Bull. Soc. Fr. Mineral. Cristallogr.*, 100:239–245.
- Wood, B. J., and Banno, S., 1973. Garnet-orthopyroxene and clinopyroxene-orthopyroxene relationships in simple and complex systems. *Contrib. Mineral. Petrol.*, 42:109–124.
- Yoder, H. S., Jr, 1976. *Generation of basaltic magma*. Washington (National Academy of Sciences), 264 p.

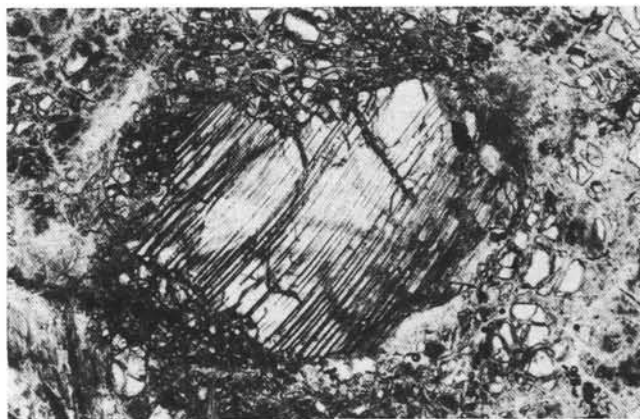
Date of initial receipt: 7 September 1988

Date of acceptance: 28 April 1989

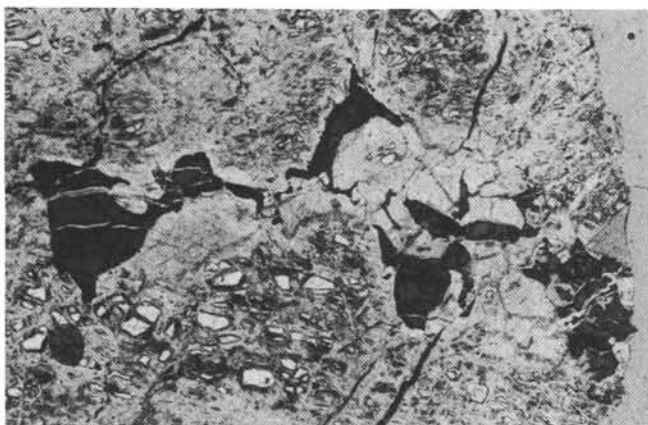
Ms 106/109B-117



1



2



3



4



5

Plate 1. 1. General view of a complete thin section, showing the typical porphyroclastic texture of one harzburgite from Site 670. One huge, deformed, and rounded opx porphyroclast, about 1 cm long, and several smaller opx and cpx porphyroclasts are included on a fine-grained olivine matrix. Sample 5R-2, 142–145 cm (#19), crossed nicols. The thin section is 35 mm long. 2. Close-up view, under microscope, of a deformed cpx porphyroclast, about 0.8 mm long, showing numerous and tiny enstatite exsolution lamellae, exsolved along (100) planes. The serpentinized olivine matrix of this lherzolite is well visible. Sample 6R-1, #8, transmitted light. Width of the picture 0.5 cm. 3. Vermicular Cr-spinels recrystallized around severely serpentinized olivine neoblasts. Sample 6R-1, 49–51 cm (#8), transmitted light. Width of the picture 0.5 cm. 4. Aspect under microscope of the olivine websterite, characterized by the abundance of deformed opx and cpx porphyroclasts, cemented by smaller opx and cpx neoblasts, and 12% interstitial olivine. This rock is remarkably fresh (about 2% serpentine and 15% secondary amphibole). Sample 9R-1, 19–20 cm (#3), transmitted light. Width of the picture 0.5 cm. 5. Macroscopic aspect of Site 670 peridotites, with their pyroxene porphyroclasts (the most brilliant ones are bastitized opx), slightly flattened and elongated along the foliation plane and included in a fine-grained, serpentinized olivine-rich matrix.